

Spatiotemporal variation and mechanisms of temperature inversion in the Bay of Bengal and the eastern equatorial Indian Ocean

K M Azam Chowdhury^{1,3,4}, Wensheng Jiang^{2*}, Guimei Liu⁴, Md Kawser Ahmed³, Shaila Akhter¹

¹ College of Oceanic and Atmospheric Sciences, Ocean University of China, Qingdao 266100, China

² Key Lab of Marine Environment and Ecology of Ministry of Education, Ocean University of China, Qingdao 266100, China

³ Department of Oceanography & International Centre for Ocean Governance (ICOG), University of Dhaka, Dhaka 1000, Bangladesh

⁴ National Marine Environmental Forecasting Center, Beijing 100081, China

Received 5 February 2021; accepted 11 June 2021

© Chinese Society for Oceanography and Springer-Verlag GmbH Germany, part of Springer Nature 2022

Abstract

In the northern Bay of Bengal, the existence of intense temperature inversion during winter is a widely accepted phenomenon. However, occurrences of temperature inversion during other seasons and the spatial distribution within and adjacent to the Bay of Bengal are not well understood. In this study, a higher resolution spatiotemporal variation of temperature inversion and its mechanisms are examined with mixed layer heat and salt budget analysis utilizing long-term Argo (2004 to 2020) and RAMA (2007 to 2020) profiles data in the Bay of Bengal and eastern equatorial Indian Ocean (EEIO). Temperature inversion exists (17.5% of the total 39 293 Argo and 51.6% of the 28 894 RAMA profiles) throughout the year in the entire study area. It shows strong seasonal variation, with the highest occurrences in winter and the lowest in spring. Besides winter inversion in the northern Bay of Bengal, two other regions with frequent temperature inversion are identified in this study for the first time: the northeastern part of the Bay of Bengal and the eastern part of the EEIO during summer and autumn. Driving processes of temperature inversion for different subregions are revealed in the current study. Penetration of heat (mean ~ 25 W/m²) below the haline-stratified shallow mixed layer leads to a relatively warmer subsurface layer along with the simultaneous cooling tendency in mixed layer, which controls more occurrence of temperature inversion in the northern Bay of Bengal throughout the year. Comparatively lower cooling tendency due to net surface heat loss and higher mixed layer salinity leaves the southern part of the bay less supportive to the formation of temperature inversion than the northern bay. In the EEIO, slightly cooling tendency in the mixed layer along with the subduction of warm-salty Arabian Sea water beneath the cold-fresher Bay of Bengal water, and downwelling of thermocline creates a favorable environment for forming temperature inversion mainly during summer and autumn. Deeper isothermal layer depth, and thicker barrier layer thickness intensify the temperature inversion both in the Bay of Bengal and EEIO.

Key words: temperature inversion, Bay of Bengal, Argo and RAMA data, intrusion of the Arabian Sea water, eastern equatorial Indian Ocean, penetrative heat below mixed layer depth

Citation: K M Azam Chowdhury, Jiang Wensheng, Liu Guimei, Ahmed Md Kawser, Akhter Shaila. 2022. Spatiotemporal variation and mechanisms of temperature inversion in the Bay of Bengal and the eastern equatorial Indian Ocean. *Acta Oceanologica Sinica*, 41(4): 23–39, doi: 10.1007/s13131-021-1873-4

1 Introduction

A warm subsurface layer sandwiched between colder surface and subsurface water layers is known as a temperature inversion layer, which is a common phenomenon in subpolar regions such as the northwestern Pacific Ocean (Nagata, 1970; Vialard and Delecluse, 1998; Ueno et al., 2005; De Boyer Montégut et al., 2007). This event is also reported from tropical oceans such as the Arabian Sea (Thadathil and Gosh, 1992; Durand et al., 2004; Shankar et al., 2004; Kurian and Vinayachandran, 2006) and the Bay of Bengal (Rao et al., 1983; Girishkumar et al., 2013; Li et al., 2016; Thadathil et al., 2002, 2016; Chowdhury et al., 2019; He et al., 2020). The exchange of heat and biogeochemical constituents

between the surface and deeper ocean is impeded where temperature inversion occurs (Godfrey and Lindstrom, 1989; De Boyer Montégut et al., 2007; He et al., 2020). Temperature inversion can play a substantial role in influencing the regional climate system by modifying the sea surface temperature (SST) and the heat content in the mixed layer (i.e., uniform density layer) (Durand et al., 2004; Balaguru et al., 2012; Thadathil et al., 2016; Kashem et al., 2019).

Previous studies have focused on the characteristics of temperature inversion and its mechanism in the Bay of Bengal (Rao et al., 1983, 1987; Suryanarayana et al., 1993; Thadathil et al., 2002, 2016; Vinayachandran et al., 2002; Li et al., 2012, 2016; Gir-

Foundation item: The Marine Scholarship of China, China Scholarship Council (CSC) for International Doctoral Students under contract No. 2017SOA016552; the National Natural Science Foundation of China under contract Nos U2106204 and 41676003.

*Corresponding author, E-mail: wjiang@ouc.edu.cn

ishkumar et al., 2013; Shee et al., 2019; He et al., 2020). However, the temporal distribution of temperature inversion in the Bay of Bengal is debated. Although most of the studies agreed on the existence of temperature inversion only during the winter (Thadathil et al., 2002, 2016; Shee et al., 2019; He et al., 2020), several studies suggested that temperature inversion also occurs during spring, summer, and autumn. For instance, Li et al. (2012) reported temperature inversion in late spring along the Sri Lankan dome, Vinayachandran et al. (2002) recognized summer temperature inversion along the northern bay, and Girishkumar et al. (2013) observed temperature inversion in the central bay from autumn through winter. Moreover, based on limited Argo data (Array for Real-time Geostrophic Oceanography), Thompson et al. (2006) and De Boyer Montégut et al. (2007) suggested that temperature inversion exists almost throughout the year in the Bay of Bengal. Thadathil et al. (2016) also reported comparatively weaker inversions in the central and southern parts of the bay at Research Moored Array for African-Asian-Australian Monsoon Analysis and Prediction (RAMA) buoy stations (12°N, 8°N, 4°N) along 90°E, which provided evidence of the temperature inversion outside the northern Bay of Bengal from the *in-situ* data.

Li et al. (2016) grasped the prominent structure of the temperature inversion in the northern Bay of Bengal during winter by analyzing the temporally and spatially averaged temperature inversion (averaged within a 2°×2° bin with a time span of 5 days) from basin-wide Argo data (approximately 20 000 profiles). However, a basin-wide detailed picture of temperature inversion other than winter season is not known which inspired us to conduct this study focusing on finer-scale temporal and spatial distribution of temperature inversion in the Bay of Bengal considering all available quality-controlled long-term Argo (2004–2020) and RAMA (2007–2020) profiles.

The net surface heat loss and the freshwater advection are suggested as the key mechanisms for the temperature inversion in the northern Bay of Bengal during winter based on studies concentrating only on portion of the bay or just a single RAMA buoy data (Li et al., 2016; Thadathil et al., 2016; Shee et al., 2019). For instance, Li et al. (2016) and Thadathil et al. (2016) studied the mechanisms of temperature inversion utilizing heat budget analysis considering the RAMA buoy at position (15°N, 90°E), and Shee et al. (2019) used data from a single Argo float. Penetrated heat below the mixed layer is also reported as a favorable mechanism for the generation of temperature inversion from autumn to winter in the central bay based on RAMA buoy located at 8°N and 90°E (Girishkumar et al., 2013). Role of downwelling eddy was proposed as one of the important mechanisms for the formation of inversion during winter along the northern bay (He et al., 2020). The above-mentioned four mechanisms of temperature inversion are either based on data from the northern portions of the bay or at a few specific RAMA buoy stations with inversion primarily during the winter. Thus, it still needs to be explored how these mechanisms works in other seasons and in the other parts of the bay.

The eastern equatorial Indian Ocean (EEIO), located just south of this bay (Fig. 1), has a strong link with the Bay of Bengal through the exchange of momentum and material, which might also influence the temperature inversion characteristics inside the bay. For example, the Bay of Bengal is remotely influenced by the wind and planetary waves generated in the EEIO (Wyrki et al., 1971; Girishkumar et al., 2011). In addition, the intrusion of warm saltier water from the Arabian Sea via the EEIO increases the salinity of the fresher water in the Bay of Bengal (Vinayachandran et al., 2013). Although Thompson et al. (2006) and De

Boyer Montégut et al. (2007) reported the year-round existence of temperature inversion in the EEIO based on limited datasets, it is still not well studied in terms of temperature inversion. Thus, in this study, in addition to the Bay of Bengal, the adjacent EEIO is also included to understand the temperature inversion (Fig. 1).

Along the southern part of the bay and the EEIO region, propagation of downwelling Rossby waves has been identified as a mechanism of temperature inversion (Thompson et al., 2006). The warm saltier Arabian Sea water slides beneath the cold-fresher continental water of the Bay of Bengal and creates a vertical thermohaline front (Shetye et al., 1993; Vinayachandran et al., 2013; Ma et al., 2019). This thermohaline front could be one of the mechanisms of temperature inversion in the study domain which is similar to the mechanism reported in Kurian and Vinayachandran (2006) in the southeastern Arabian Sea that the fresher water from the Bay of Bengal flows above the warm saltier water there. Moreover, the four proposed mechanisms for the Bay of Bengal listed above also need to be explored for the EEIO. In short, it is obvious that our understanding of relative contributions from various mechanisms responsible for temperature inversion in the Bay of Bengal and EEIO is yet to be apprehended and thus, attempted to address it in this study.

The paper is arranged as follows. In the next section, data sources and methods are described briefly. Section 3 outlines the detailed structure of the basin-wide seasonal cycle of the temperature inversion and the associated driving forces. Finally, the summary and conclusions are stated in Section 4.

2 Materials and methods

Both observational (temperature and salinity profiles) and reanalysis datasets (atmospheric heat fluxes, freshwater fluxes, and wind fields) are used in this study. To avoid erroneous data, a quality control procedure of the utilized Argo data is carried out. In this study, based on the annual cycles of the heat and freshwater fluxes, 4 seasons are considered as follows: winter (Decem-

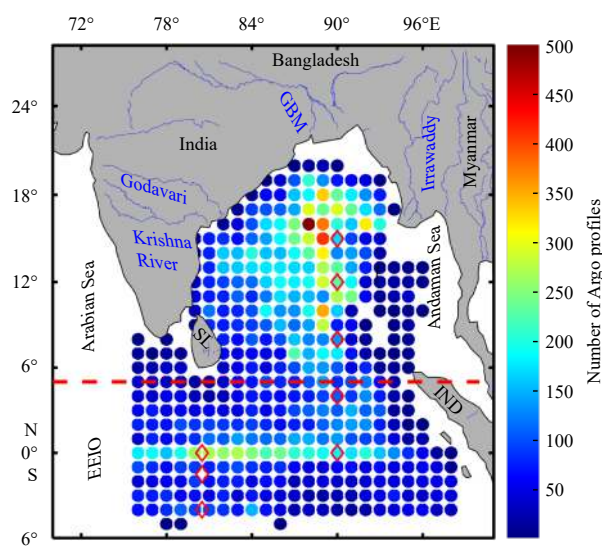


Fig. 1. The number distribution of Argo profiles at 1°×1° grid in the Bay of Bengal and the eastern equatorial Indian Ocean (EEIO). The red dashed line is the boundary between the Bay of Bengal and the EEIO. The eight RAMA mooring buoy are marked by the red diamonds. GBM is short for the Ganges-Brahmaputra-Meghna Rivers; SL is short for the country name Sri Lanka; and IND is for Indonesia.

ber–February), spring (March–May), summer (June–September), and autumn (October–November), pursuing Thadathil et al. (2007) and Shee et al. (2019).

2.1 Data sources

2.1.1 Temperature and salinity profiles

Temperature (°C) and salinity data of Argo profiling floats (Argo, 2021) in the Bay of Bengal and the EEIO are downloaded from the Global Ocean Data Assimilation Experiment project website (<http://www.argo.ucsd.edu>) spanning from 2004 to 2020. The spatial distribution of Argo floats (counted in a 1°×1° grid) in the study area (5°S–23°N, 76°–100°E) is shown in Fig. 1.

Observational temperature profiles from RAMA buoy are utilized to describe and understand the occurrence of temperature inversion. Data from the eight RAMA buoys (marked as diamond in Fig. 1) located in the Bay of Bengal ((15°N, 90°E), (12°N, 90°E), (8°N, 90°E)), and EEIO ((4°N, 90°E), (0°N, 90°E), (0°N, 80.5°E), (1.5°S, 80.5°E), and (4°S, 80.5°E)) over 2007 to 2020 are utilized. These buoys provide daily time series of temperature profiles collected at 1 m, 10 m, 13 m, 20 m, 40 m, 60 m, 80 m, 100 m, 120 m, 140 m, 180 m, 300 m, and 500 m depths. Some of these daily profiles missed some data at different depths. Thus, profiles with missing data at more than two consecutive depths are excluded from the analysis. Finally, each profile is linearly interpolated with 1-m depth interval.

2.1.2 Heat flux, freshwater flux, wind speed, and surface current data

The ERA-Interim reanalysis dataset produced by the European Centre for Medium-range Weather Forecast (ECMWF) is used in this study to reveal the mechanism of temperature inversion. The monthly mean wind speed (m/s), zonal and meridional components of wind velocity at 10 m above ground, precipitation (depth in meters of water equivalent), evaporation (depth in meters of water equivalent), shortwave radiation (W/m²), and surface net heat flux (W/m²) are taken from ECMWF data. The sea surface current fields derived from the Ocean Surface Current Analysis (OSCAR) ((1/3)° resolution) (https://podaac.jpl.nasa.gov/dataset/OSCAR_L4_OC_third-deg) are utilized here. All data are taken for the years 2004 to 2020.

2.2 Methods

2.2.1 Quality control of Argo data

Initially, all available data (approximately 54 000 Argo profiles) from 2004 to 2020 are considered. To find the best quality data, at the first step of quality control, only those data marked as “flag 1” are selected (Wong et al., 2021). Then, from the selected dataset, only the profiles with depths of 5 m and deeper are considered, since the data in Argo float near the surface are generally discouraged from use in scientific studies (after Wong et al., 2021). Generally, temperature inversion occurs within 5 m to 120 m (Vinayachandran et al., 2002; Thompson et al., 2006; Thadathil et al., 2016). Thus, profiles with starting depths greater than 5 m or ending depths less than 120 m are excluded from the analysis. Finally, profiles with temperature ranging below 5°C or above 35°C or salinity ranging below 20 or above 37 are removed. Eventually, after quality control, the number of Argo profiles are reduced from 54 000 to 39 293. Then, the data of each profile are linearly interpolated with a 1-m depth interval starting from 5-m depth to the end of the profiles.

2.2.2 Defining the temperature inversion and related parameters

To define the temperature inversion, it is important to fix a temperature threshold (the minimum increase in temperature in the subsurface). In recent studies, both 0.1°C (Girishkumar et al., 2013; Thadathil et al., 2016; Shee et al., 2019) and 0.2°C (Thompson et al., 2006; De Boyer Montégut et al., 2007; Li et al., 2016) temperature thresholds were used to define temperature inversions in the Bay of Bengal and the EEIO. To capture the temperature inversion, definitely 0.2°C is chosen in this study to be the threshold. The accuracy of the temperatures in the Argo profiles is <http://argo.ucsd.edu/>, which is much lower than our chosen threshold (0.2). If any Argo profile does not show a minimum temperature increment of 0.2, then the profile is considered a noninversion profile. The temperature, salinity, and density at a depth of 5 m taken from Argo profiles are considered to be SST, sea surface salinity (SSS), and sea surface density, respectively. For convenience, the sea water density is presented in terms of σ_t (i.e., sea water density minus 1 000) (Figs 2a, b).

The decrease in temperature by 1°C from the surface to the subsurface is set as the criterion to determine the isothermal layer depth (ILD, the layer with uniform temperature) for the noninversion case (Wyrteki et al., 1971; Sprintall and Tomczak, 1992; Masson et al., 2002; Rao and Sivakumar, 2003; Thadathil et al., 2007, 2016; Shee et al., 2019) (Fig. 3a). In the northern bay, subsurface increases in temperature of approximately 3°C to 4°C are quite common during winter in inversion profiles (Thadathil et al., 2002). Thus, a surface temperature drops of 1°C to calculate ILD provides an overestimation of an average 20 m in temperature inversion profiles (Fig. 3a), which is also pointed out by Thadathil et al. (2007). In this case, Thadathil et al. (2007) regarded the surface as the upper limit of ILD, and the depth at which the temperature reaches that SST again is the lower limit of ILD (hereafter, named the repeat of SST criteria) (Fig. 3a). In this study, the definition used by Thadathil et al. (2007) of ILD is adopted for the inversion case.

The water density calculated from Argo temperature and salinity data is used to calculate the mixed layer depth (MLD, a bottom depth of the mixed layer). The increase in surface density by 0.125 kg/m³ or 0.2 kg/m³ has been used as the fixed density criterion (hereafter, named the method 1, see Fig. 3b) to determine the MLD for both inversion and noninversion profiles (Monterey and Levitus, 1997; Girishkumar et al., 2013; Thadathil et al., 2002, 2016). However, to maintain consistency with the definition of ILD, MLD (see Eq. (1)) is also calculated in terms of depth with a density equals to that at the surface plus an increment in density equivalent to the decrease in temperature by 1°C (hereafter, named the method 2, see Fig. 3b) (Kara et al., 2000; Rao and Sivakumar, 2003; De Boyer Montégut et al., 2004; Thadathil et al., 2007; Kumari et al., 2018; He et al., 2020). Both MLD definitions generate almost similar results (i.e., difference is less than 3 m; Fig. 3b), and finally, the latter one is adopted for all types of profiles in this study. Hence, the increment of the density is as follows:

$$\Delta\sigma = \sigma_t(\text{SST} + dT, \text{SSS}, P_0) - \sigma_t(\text{SST}, \text{SSS}, P_0), \quad (1)$$

where $\Delta\sigma$ is the density difference between the surface and the MLD; σ_t is the potential density (kg/m³) calculated from the temperature, salinity and reference pressure (P_0); and dT is a 1°C temperature increase.

The depth where the subsurface temperature has just exceeded the SST by 0.02°C is defined as the initial inversion depth

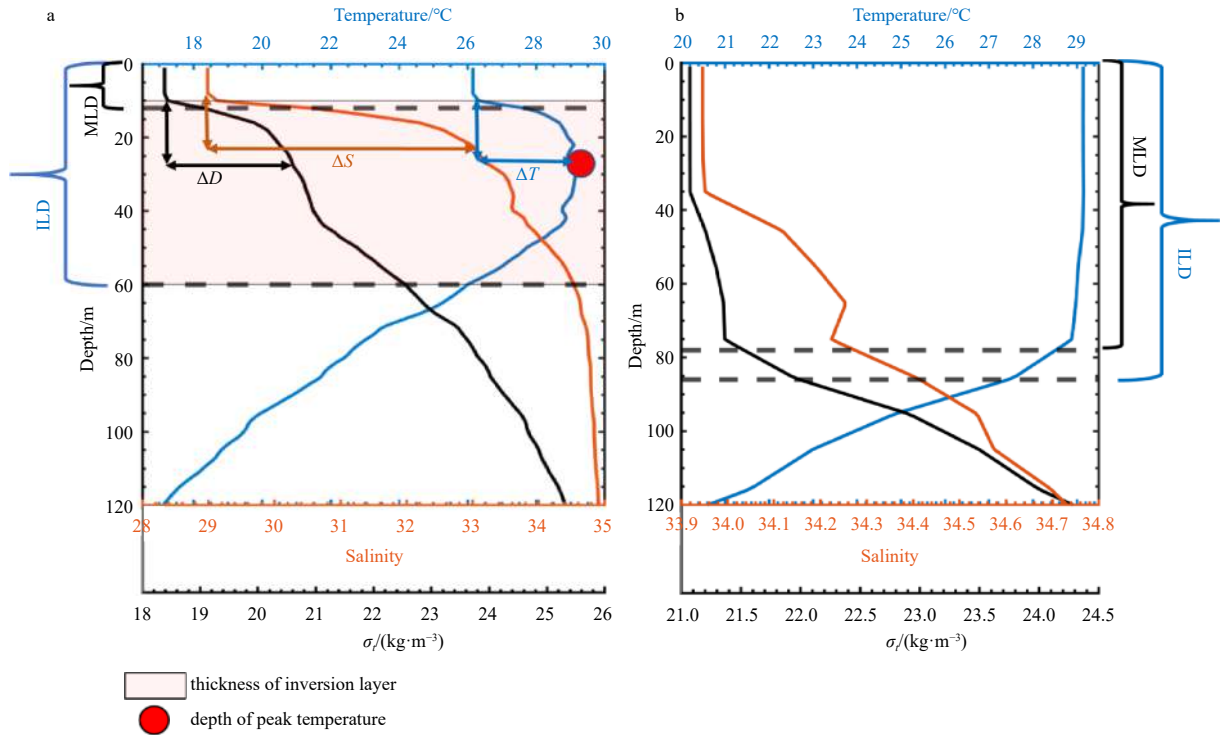


Fig. 2. Pictorial presentation of different parameters related to temperature inversion (a), and non-inversion (b) profiles. MLD: mixed layer depth; ILD: isothermal layer depth.

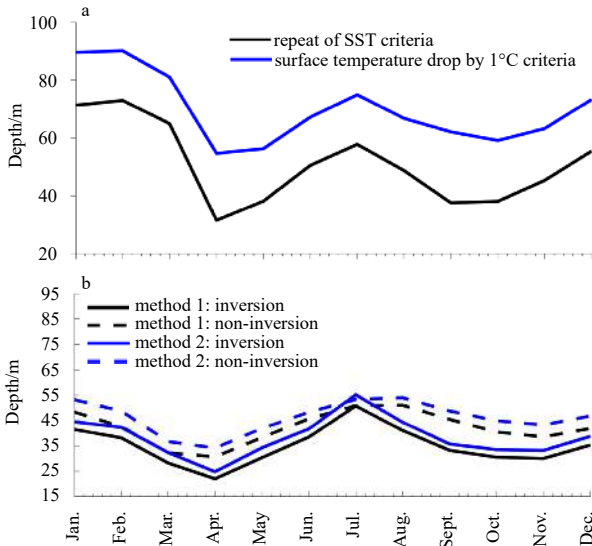


Fig. 3. Monthly variations in ILD (a), and mixed layer depth (b) using two different calculation methods.

(i.e., starting depth of the temperature inversion). The layer between the initial inversion depth and the bottom of the ILD is termed the temperature inversion layer (Fig. 2a, shaded regions). The intensity of the temperature inversion is determined by the thickness of the temperature inversion layer (hereafter, the thickness of the inversion layer), the depth of the peak temperature (i.e., the depth where the subsurface temperature reaches the maximum), and the temperature at the depth of the peak temperature. ΔT is the temperature difference between the value of peak temperature and SST, while ΔS and ΔD are the salinity and density difference between the corresponding value at the depth

of peak temperature and at the surface, respectively (Fig. 2a).

2.2.3 Determining the water column stratification

The Brunt-Väisälä frequency is the formal measure of the stratification tendency in a water column. This frequency is calculated for both temperature inversion and noninversion profiles using the following equation (Roseli et al., 2015):

$$N^2 = -\frac{g \Delta \rho}{\rho \Delta z}, \quad (2)$$

where N is Brunt-Väisälä frequency; g is gravitational acceleration; ρ is potential density; $\Delta \rho$ is difference between potential densities of two water parcels; and Δz is the vertical distance of the two water parcels. If $N^2 > 0$, the stratification is stable and does not overturn locally.

2.2.4 Mixed layer heat budget analysis method

The heat budget at each grid point in the basin can be described by the following equation:

$$\frac{dT}{dt} = \frac{Q_{\text{net}} - Q_{\text{pen}}}{\rho C_p h} - \left(u \frac{\partial T}{\partial x} + v \frac{\partial T}{\partial y} \right) + H[(W_{d23} + \partial_t h)] \frac{(T_{h+5} - T_h)}{h} + \frac{K_z}{h} \partial_z T + \text{remainder}. \quad (3)$$

In this equation, six terms are included in the balance. Different terms in the mixed layer heat budget analysis can contribute to the temperature change in the mixed layer and hence help to explain the temperature inversion process (Thadathil et al., 2016; Li et al., 2016; Girishkumar et al., 2013).

Term (a) represents the basin-averaged mixed layer temperature tendency, where T is the mixed layer temperature at each grid point calculated from Argo temperature profiles and $\frac{dT}{dt}$ is the rate of change of T with respect to month. Term (b) represents the mixed layer heat flux, where (Q_{pen}) is the penetrated component of solar radiation below the MLD; Q_{net} is the net atmospheric heat flux; ρ is the seawater density (as a function of depth) calculated from temperature and salinity profiles; C_p (3 989.2 J/(kg·°C)) is the specific heat capacity of seawater, and h is the MLD. Q_{pen} is estimated as follows:

$$Q_{pen} = 0.47 \times Q_{short} \left(\nu_1 e^{-\frac{h}{\zeta_1}} + \nu_2 e^{-\frac{h}{\zeta_2}} \right), \quad (4)$$

where incoming shortwave radiation (Q_{short}) is corrected for albedo at the sea surface (downwelling shortwave radiation is multiplied by 0.945). ν_1 and ν_2 are the partitioning factors (with $\nu_1 + \nu_2 = 1$). ζ_1 and ζ_2 are the attenuation depths of long visible, short visible and ultraviolet wavelengths (Morel and Antoine, 1994; Sweeney et al., 2005). The approximate values of ν_1 , ν_2 , ζ_1 and ζ_2 are 0.39, 0.69, 1.52, and 18.9, respectively (Morel and Antoine, 1994; Girishkumar et al., 2013).

Term (c) is called the horizontal advection term (temperature), and u and v are the zonal and meridional components of the surface current. x and y indicate the longitudinal direction and latitudinal direction, respectively. Thus, the horizontal advection term is the combination of the longitudinal and latitudinal components of the surface current and its transport.

Term (d) represents the vertical advection and vertical entrainment. W_{d23} is the vertical velocity (m/month), which is the time rate of change of the 23°C isotherm depth (an indicator of thermocline depth in the Bay of Bengal, Girishkumar et al., 2013) and it is determined between MLD and 5 m below the mixed layer (i.e., MLD+5). $\partial_t h$ is the time rate of change of MLD. The combination of W_{d23} and $\partial_t h$ is the resultant entrainment velocity (m/month) at the bottom of the mixed layer. H is the Heaviside step function [$H=0$ if $(W_{d23} + \partial_t h) < 0$, $H=1$ if $(W_{d23} + \partial_t h) > 0$]. Term (e) represents the vertical diffusion. $\partial_z T$ is the average vertical temperature gradient between the base of mixed layer and 5 m below the MLD; the vertical diffusion coefficient, K_z is considered to be 1 cm²/s. Hereafter, vertical advection, entrainment and diffusion (i.e., terms (d) and (e)) are combinedly designated to be the vertical processes for convenient representation in this study.

Finally, term (f) is called as a remainder, which might contain measurement errors related to horizontal currents and surface heat fluxes, errors in parameterizing vertical processes, computational errors associated with finite differencing, and sampling errors (Foltz and McPhaden, 2009; Vialard et al., 2008; Halkides and Lee, 2011; Thadathil et al., 2016).

2.2.5 Mixed layer salt budget analysis method

There are also several terms in the mixed layer salt budget, which are also important for describing the mechanism of temperature inversion (Li et al., 2016). The salt budget equation calculated at each grid point for the basin is as follows:

$$\frac{dS}{dt} = \frac{(E-P)S}{h} - \left(u \frac{\partial S}{\partial x} + v \frac{\partial S}{\partial y} \right) + H[(W_{d23} + \partial_t h)] \frac{(S_{h+5} - S_h)}{h} + \frac{K_z}{h} \partial_z S + \text{remainder}. \quad (5)$$

In this equation, term (a) represents the basin-averaged mixed layer salinity tendency calculated from Argo salinity profile data, where S is the mixed layer salinity and $\frac{dS}{dt}$ is the rate of change of S with respect to month. Term (b) represents the mixed layer fresh-water flux term, where E , P , and S are the evaporation, precipitation, and salinity at each grid in this basin, respectively. Term (c) is called horizontal advection (salinity). Other terms (d-f) and parameters have similar meanings with Eq. (3) but for salinity, as explained in Section 2.2.4. To calculate those terms, all the atmospheric heat and fresh-water flux-related data are used from the ECMWF dataset, and surface current data are taken from the OSCAR data sources as described in Section 2.1.2.

2.2.6 Wind turbulent kinetic energy

The turbulent kinetic energy (W/m²) changes the mixing in the upper ocean that arises from the effect of momentum flux due to wind stress (Shankar et al., 2016; He et al., 2020), and thus, the characteristics of temperature inversion would also be changed owing to this turbulent kinetic energy. The wind turbulent kinetic energy is described below following He et al. (2020):

$$\text{wind turbulent kinetic energy} = \tau \sqrt{\tau / \rho}, \quad (6)$$

where τ is the magnitude of wind stress and ρ is the density of seawater.

3 Results and discussion

The detailed spatiotemporal distribution and characteristics of the temperature inversion are described in Section 3.1 (Figs 4 and 5; Tables 1 and 2). The factors responsible for the formation of the temperature inversion are discussed in the subsequent section utilizing the analysis of the mixed layer heat and salt budget, including the effects of the vertical intrusion of freshwater, warm-salty Arabian Sea water, downwelling of thermocline, wind turbulent kinetic energy, and penetrated heat below the MLD (Figs 6–13).

3.1 Spatiotemporal distribution and characteristics of temperature inversion

Temperature inversion profiles demonstrate notable spatiotemporal variation in the Bay of Bengal and the EEIO region (Fig. 4). The characteristics of the temperature inversion can be explained by the ΔT , initial inversion depth, depth of peak temperature, and thickness of the inversion layer. Similar to the temperature inversion, these parameters also exhibit significant seasonal and spatial variation in the study domain (Fig. 5, Table 1). The number of temperature inversion profiles is 6 876 (17.5 %) of the total 39 293 Argo profiles over 2004 to 2020. In RAMA daily data, the number of profiles having temperature inversion is 14 909 (51.6%) of the total 28 894 profiles from 2014 to 2020 (Table 2). Temperature inversion from Argo exhibits that the seasonal variation (standard deviation ~7%) is stronger than the inter-annual variations with standard deviation of 4.1%.

3.1.1 Temperature inversion during winter

In winter, temperature inversion is generally widespread throughout the study area, although the number of profiles with inversion decreases significantly in the southernmost portion of the bay and the EEIO. Both Argo and RAMA profiles are exhibiting this spatial distribution of inversion (Fig. 4a, Table 2). The rate of temperature inversion (55.2% of the total inversion profiles from Argo and 44.3% from RAMA) is highest during winter,

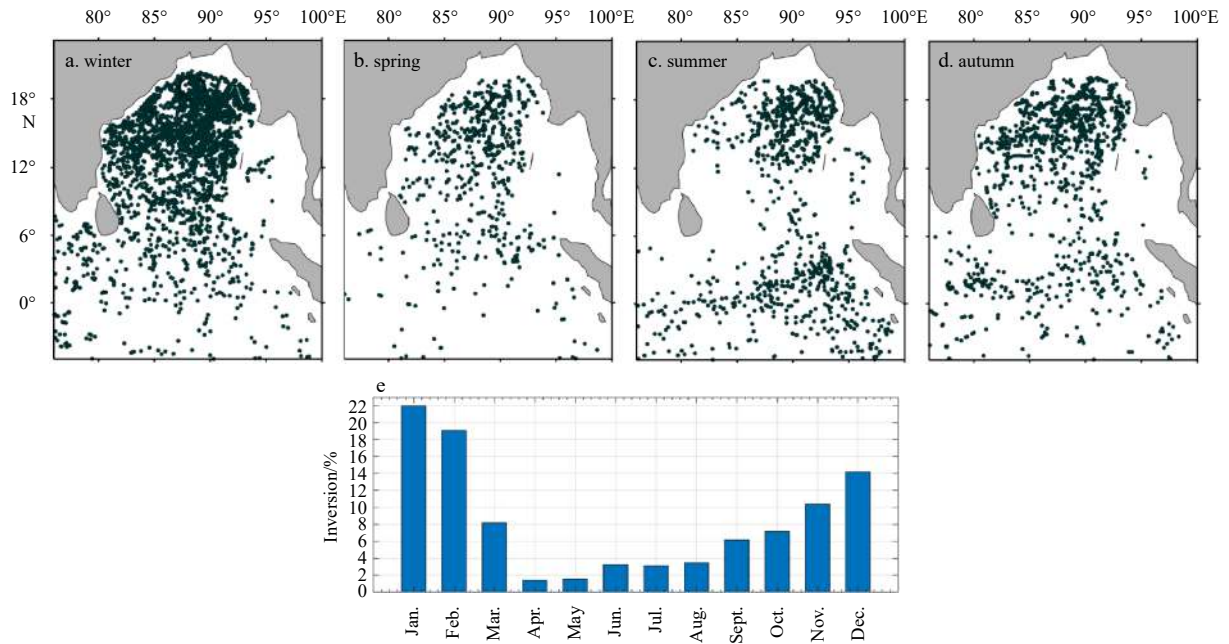


Fig. 4. Distribution of temperature inversion profiles in various seasons over 2004 to 2020 (a–d), and monthly percentages of temperature inversion profiles (e).

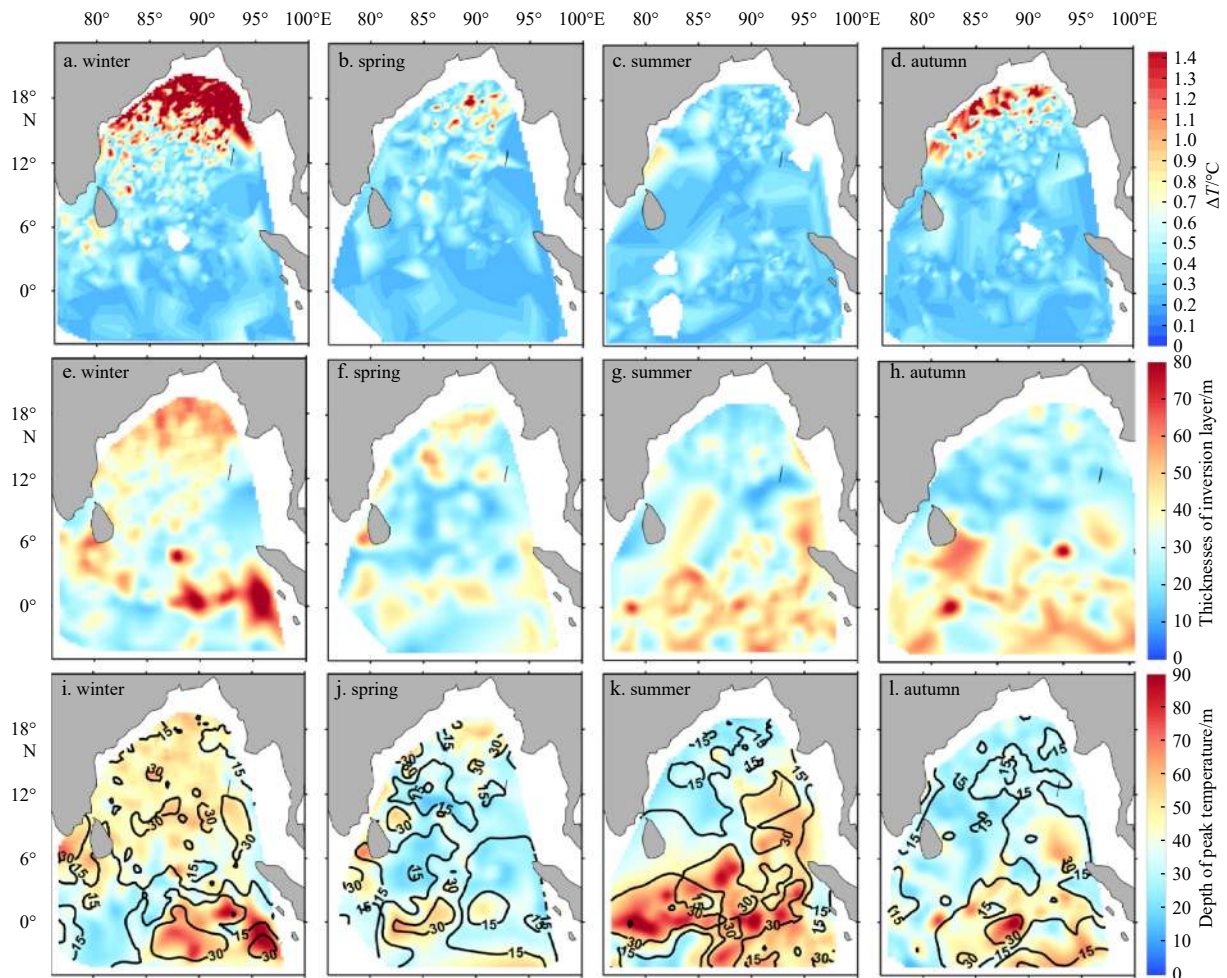


Fig. 5. Season-wise spatial distribution of ΔT (a–d), thicknesses of inversion layer (e–h), and depth of peak temperature with the contours of initial inversion depth (i–l).

Table 1. Basin averaged monthly mean of different characteristic parameters of temperature inversion derived from Argo data

Parameters	Jan.	Feb.	Mar.	Apr.	May	Jun.	Jul.	Aug.	Sept.	Oct.	Nov.	Dec.
Inversion profiles	1 518	1 316	567	98	106	226	214	239	427	496	718	978
Inversion/%	22.0	19.1	8.2	1.4	1.5	3.3	3.1	3.5	6.2	7.2	10.4	14.2
$\Delta T/^\circ\text{C}$	1.6	1.3	0.7	0.4	0.3	0.4	0.3	0.5	0.3	0.4	0.6	0.9
Initial inversion depth/m	19.4	20.9	21.6	11.1	17.3	22.9	29.3	21.5	16.5	14.9	14.8	18.0
Depth of peak temperature/m	52.9	54.7	48.8	21.2	31.4	41.5	53.5	43.5	33.1	30.4	34.6	42.6
Thickness of the inversion layer/m	52.2	52.6	43.2	19.4	23.2	28.1	34.5	35.1	27.0	26.1	31.1	38.5

Table 2. Temporal mean over 2007 to 2020 of different characteristic parameters of temperature inversion, and seasonal distribution of inversion in different RAMA buoy positions

RAMA position	Total profiles	Percentage of total TI/%	Mean $\Delta T/^\circ\text{C}$	Mean DPT/m	Winter/%	Spring/%	Summer/%	Autumn/%
0°, 80.5°E	3 511	2.2	0.32	51.7	24.7	7.2	47.4	20.6
0°, 90°E	3 612	2.3	0.28	55.7	23.2	8.5	26.8	41.5
1.5°S, 80.5°E	4 236	3.3	0.42	27.6	25.4	15.6	32.0	27.0
4°S, 80.5°E	3 513	1.5	0.34	29.5	20.8	22.6	28.3	28.3
4°N, 90°E	2 282	3.9	0.36	35.5	48.9	13.3	6.7	31.1
8°N, 90°E	2 910	6.1	0.35	48.4	70.4	10.6	2.8	16.2
12°N, 90°E	4 611	7.8	0.38	47.5	70.7	12.0	8.4	8.9
15°N, 90°E	4 219	24.5	0.73	44.4	70.6	6.2	10.9	12.3

Note: TI stands for temperature inversion and DPT stands for depth of peak temperature. Temperature inversion along EEIO during summer and autumn, and along the Bay of Bengal during winter are remarkable, and thus, shown to be “bold italic” faces.

with the maximum in January (Tables 1 and 2). Thadathil et al. (2016) also reported that the maximum inversion occurs during January at the northernmost RAMA station (15°N, 90°E).

ΔT , the difference in peak temperature and SST, increases northward and is highest during winter compared with the other seasons (Fig. 5a). The basin-wide mean ΔT is $\sim 1.3^\circ\text{C}$ (Table 1), but in some areas, it exceeds 4°C . In winter, temperature inversion starts at a deeper level, where it ranges from approximately 15 m to 35 m in the Bay of Bengal and 15 m to 40 m in the EEIO (Fig. 5i). The initial inversion depth increases from coast to offshore in the Bay of Bengal and the equatorial region, especially in the eastern EEIO (Fig. 5e). The basin-wide mean thickness of the inversion layer in winter is 48 m, which is higher than that in the other seasons (Table 1). The depth of the peak temperature and thickness of the inversion layer demonstrate a spatial correlation with the initial inversion depth (Figs 5e, i).

3.1.2 Temperature inversion during spring

The number of inversion profiles is the lowest during spring, which is approximately 11.2% of the total inversion profiles recognized during this study and distributed sparsely in the basin with a minimum in the EEIO region (Fig. 4b). During this season the lowest number of inversion ($\sim 12\%$) is also observed in the profiles of RAMA buoys. The basin-wide mean ΔT is approximately 0.47°C (Table 1), with a higher ΔT along the northeastern part of the bay (maximum $\sim 1.2^\circ\text{C}$; see Fig. 5b). The initial inversion depth (~ 10 m to 25 m), depth of peak temperature (~ 20 m to 50 m), and thickness of the inversion layer (~ 10 m to 40 m) are shallower in the northern bay and the EEIO than in the other seasons (Figs 5f, j).

3.1.3 Temperature inversion during summer and autumn

During summer and autumn, the percentages of basin-averaged temperature inversion profiles from Argo are 16.1% and 17.6%, respectively, while from RAMA buoy they are 20.4% and 23.2%, respectively. Temperature inversion profiles are densely populated along the northeastern part of the bay (Figs 4c–e). Their distribution extends toward the northwestern bay during

autumn along the path of the East Indian Coastal Current (see Shetye et al. (1996) and Chaitanya et al. (2014) for the distribution of the East Indian Coastal Current). The number of inversion profiles during these seasons is higher than that in the other seasons in the EEIO region, with more populations on the eastern side. Almost no temperature inversion profile exists in the southwestern Bay of Bengal surrounding the Sri Lankan dome during summer. The data of five RAMA buoys located in the EEIO also show that the number of temperature inversion is higher during these seasons (58%) than winter (28.6%) and spring (13.4%) (Table 2).

The basin-averaged ΔT is 0.4°C and 0.5°C during summer and autumn, respectively. However, ΔT is higher (maximum $\sim 1.4^\circ\text{C}$) along the northernmost part of the bay during autumn (Figs 5c, d). The initial inversion depth (~ 10 m to 30 m), the depth of peak temperature (~ 30 m to 90 m), and the thickness of the inversion layer (~ 20 m to 80 m) are deeper along the equatorial region and decrease gradually northward during these seasons (Figs 5g, h, k, l).

In summary, the temperature inversion occurs throughout the year in both the Bay of Bengal and the EEIO. The number of inversion profiles is minimal in spring, which gradually increases during summer and autumn and becomes the highest in winter (Fig. 4e, Tables 1 and 2). Throughout the year, Argo profiles with inversion are denser in the northern Bay of Bengal compared with the southern bay and the EEIO; however, in summer, inversion profiles become equally prevalent in the EEIO region as in the northern bay (Fig. 4). Notably, both Argo and RAMA profiles exhibit that the occurrence of inversion in the EEIO is higher during summer and autumn than other seasons. The existence of the finer scale temperature inversion from spring to autumn in the Bay of Bengal and throughout the year in the EEIO is a novel finding.

3.2 Driving forces for the formation of temperature inversion

The basin-averaged mixed layer temperature (annual average $\sim 28.7^\circ\text{C}$) and salinity (annual average ~ 32.9) in the temperature inversion profiles are substantially lower than those in the non-inversion profiles (temperature $\sim 29.0^\circ\text{C}$, salinity ~ 33.8) (Figs 6i, j). Both the mixed layer temperature ($r = -0.91$) and salinity ($r = -0.54$)

have significant correlations with the number of inversion profiles (Table 3). Low mixed layer temperature and salinity are necessary to form the temperature inversion, and thus, factors that control mixed layer temperature and salinity conditions may also have a significant influence on the formation of the temperature inversion layer (De Boyer Montégut et al., 2007; Thadathil et al., 2016; Li et al., 2016; Chowdhury et al., 2017; Shee et al., 2019). Hence, the mixed layer heat and salt budget analysis are separately presented for the northern Bay of Bengal (15°N), southern Bay of Bengal (5°N to 15°N) and the EEIO region to find out the contributions of different components to the mixed layer temperature and salinity tendency in each region (Figs 7i–n).

3.2.1 The Bay of Bengal

Along the northern Bay of Bengal, both the mixed layer temperature (25.5°C to 28.0°C) and salinity (31.0 to 33.5) reach their lowest values in winter (Figs 6b, f), when the amount of temperature inversion is the highest. During this period, evaporation dominates over precipitation (Fig. 7f), which can also be found from the positive fresh-water flux (calculated using Eq. (5)) depicted in Fig. 7j. However, the river discharge that results from

high precipitation in summer reaches the bay during autumn with a time lag that continues to flow in during winter (Akhil et al., 2014; Chaitanya et al., 2014; Pant et al., 2015) helps to maintain a lower mixed layer salinity despite the positive evaporation minus precipitation (E–P). The negative horizontal salinity advection (~ -0.5) also supports this phenomenon (Fig. 7j). Moreover, the 32.5-isohaline depth (as a proxy of the vertical intrusion of freshwater) of the temperature inversion profile occurs at a deeper depth (mean ~ 28 m) in the region of low saline water in winter (Fig. 8a) and makes the upper layer strongly stratified (Fig. 8b), which yields high ΔS (1.0 to 3.5) (Fig. 8d).

Salty water from the Arabian Sea intrudes into the Bay of Bengal throughout the year (Vinayachandran et al., 2013). The 35-isohaline depth (as a proxy of salty water, Vinayachandran et al., 2013) along with the salinity contours at 50-m depth (to see subsurface salinity pattern) exhibits the plume of salty Arabian Sea water from the southwestern part of the study domain, slides beneath the comparatively low saline surface water of the Bay of Bengal (Figs 9a–d). This sliding salty water reaches approximately 250 m of depth along the northern Bay of Bengal during winter (Fig. 9b). The intruding high-salinity water creates

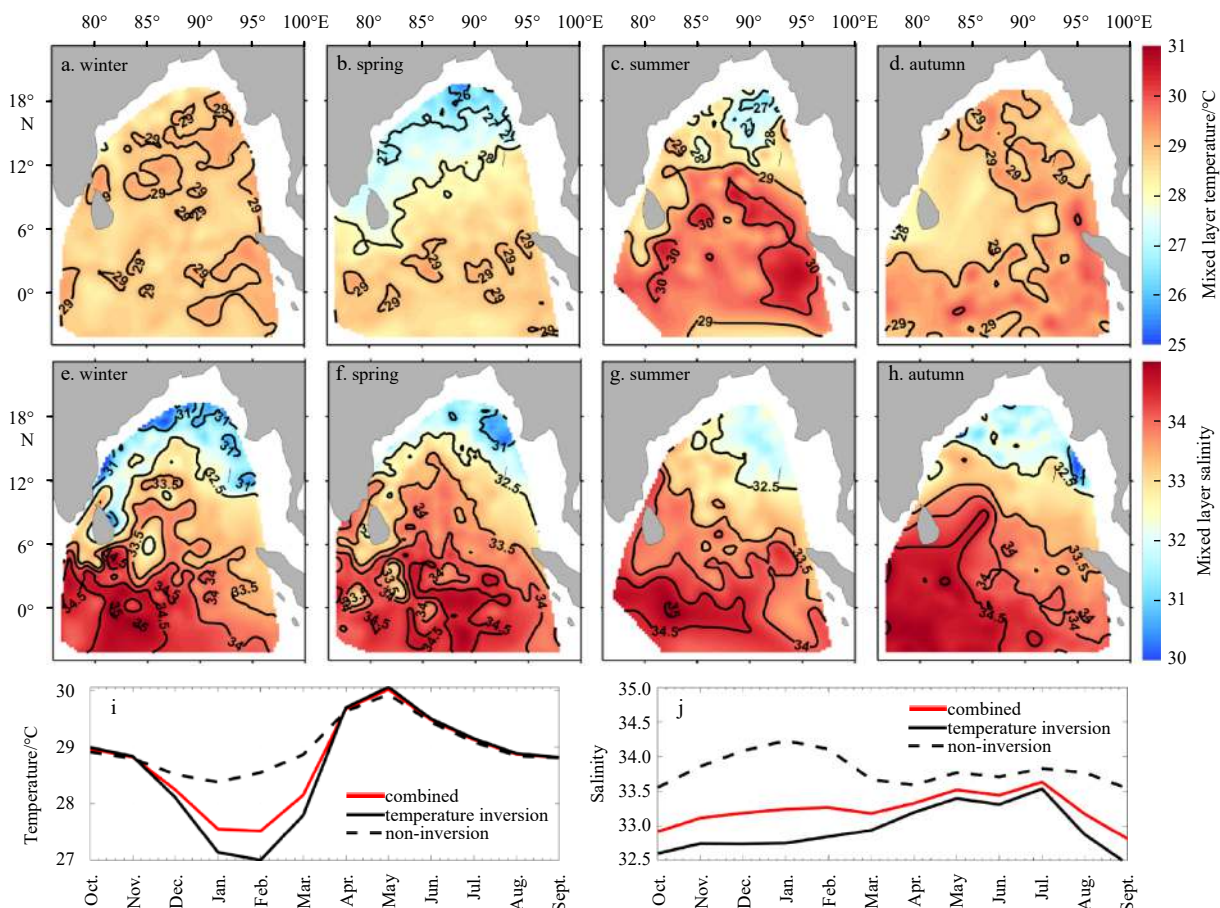


Fig. 6. Spatial distribution of the mixed layer temperature (a–d), mixed layer salinity (e–h) of temperature inversion profiles, and monthly variation in mixed layer temperature (i), and mixed layer salinity (j).

Table 3. Correlation between the number of temperature inversion with associated parameters in the study domain

	MHF	NHF	MLT	MFWF	E–P	MLS	ΔS	ΔD	32.5 isohaline	W.TKE
Number of temperature inversion	<i>-0.76</i>	<i>-0.79</i>	<i>-0.91</i>	0.41	<i>0.46</i>	<i>-0.54</i>	<i>0.94</i>	<i>0.70</i>	0.44	<i>-0.42</i>

Note: MHF, NHF, MLT, MFWF, MLS, and W.TKE represent mixed layer heat flux, net surface heat flux, mixed layer temperature, mixed layer fresh-water flux, mixed layer salinity, and wind turbulent kinetic energy, respectively. More than 95% significant correlations are shown to be “bold italic” faces.

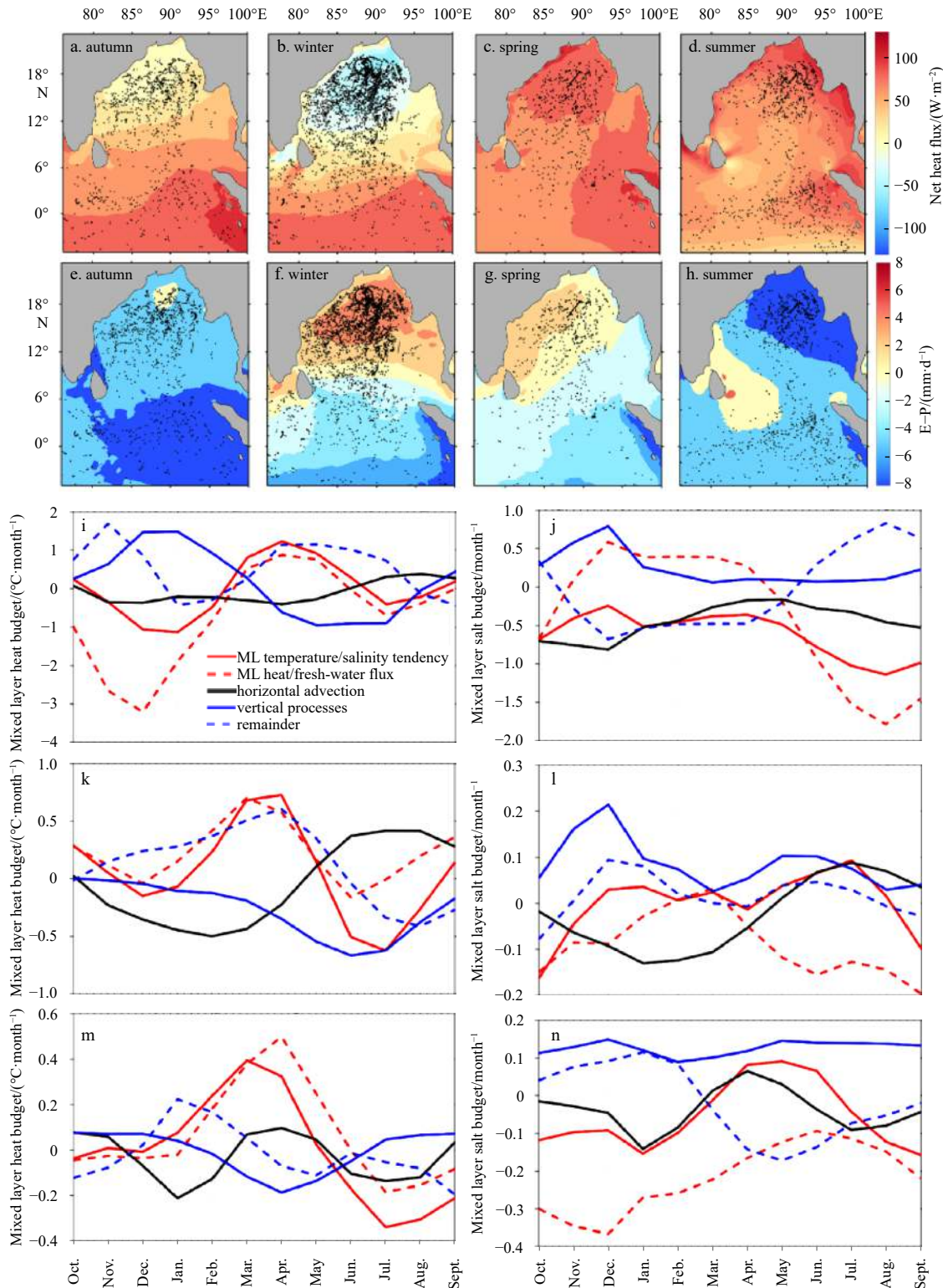


Fig. 7. Spatiotemporal distribution of net surface heat flux (a–d), and E–P (e–h). Black dots refer to the location of temperature inversion profiles. Mixed layer (ML) heat budget and salt budget in the northern Bay of Bengal (i, j), southern Bay of Bengal (k, l), and EEIO (m, n), respectively.

stronger salinity stratification with the overlying low-saline water and helps in producing a higher ΔS in this bay (Figs 8c–f). The high ΔS results in a shallower mixed layer (Thadathil et al., 2002; De Boyer Montégut et al., 2007) and a thick barrier layer, which stays just below the MLD (Mignot et al., 2012). Depth of 26°C iso-

therm becomes deeper (~ 75 m) during this season in the Bay of Bengal (Fig. 10b), and it is said to be favorable for the formation of intense temperature inversion (He et al., 2020). The wind turbulent kinetic energy along the northern bay is comparatively weaker in this season (Fig. 11b). Thus, wind-induced mixing re-

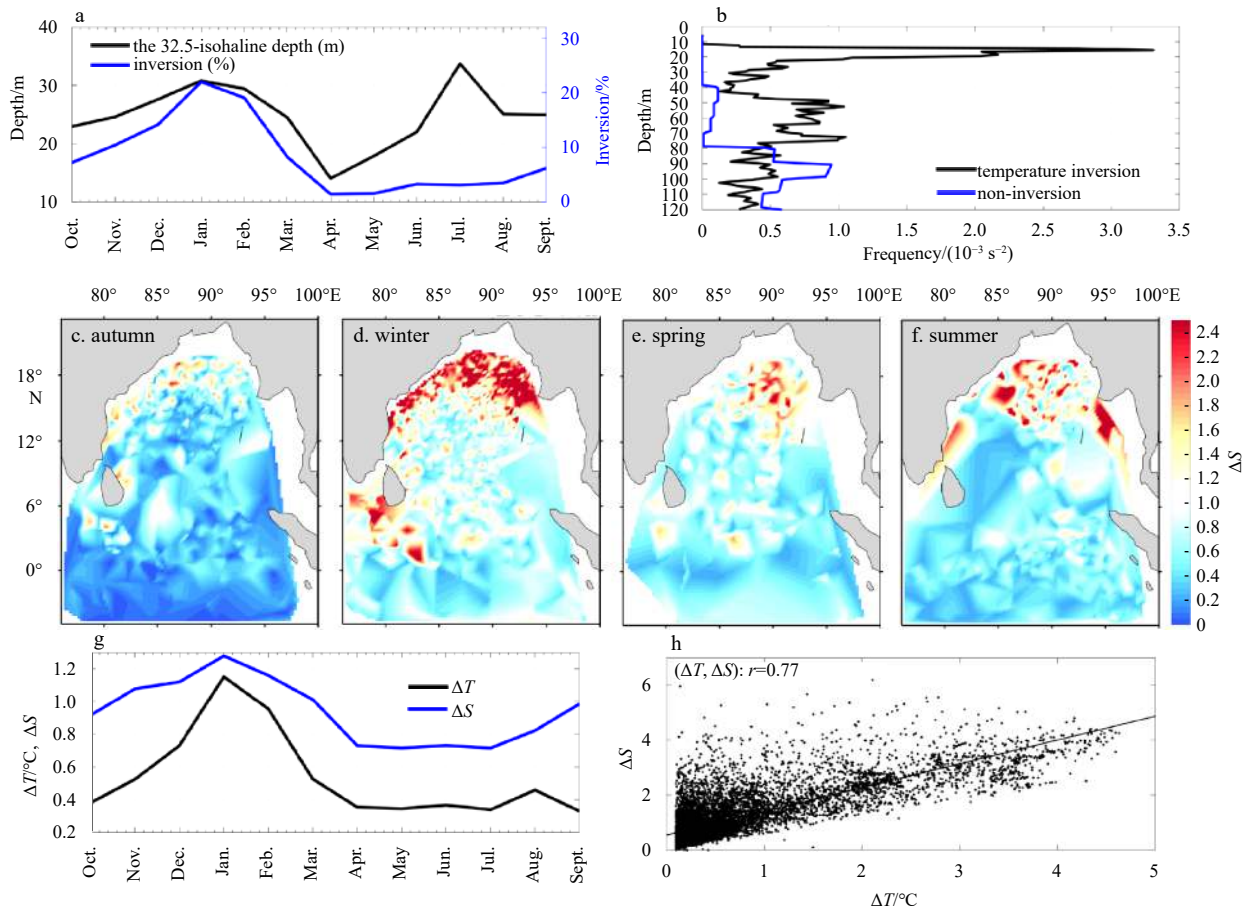


Fig. 8. Basin averaged monthly variation of the 32.5-isohaline depth and the percentages of temperature inversion (a), water column stratification (s^{-2}) in temperature inversion and non-inversion profiles (b), spatiotemporal distribution of ΔS (c-f), monthly variation of ΔT and ΔS (g), and their correlations (h).

stricts within the shallow MLD and cannot influence the underneath barrier layer (Luis and Kawamura, 2000; Kurian and Vinayachandran, 2006; He et al., 2020), which might be favorable to form the temperature inversion.

The incoming solar radiation penetrating below the shallow mixed layer reaches into the barrier layer and warms this layer (Schiller and Godfrey, 2003; Kurian and Vinayachandran, 2006). If the warming in the subsurface layer of the ocean becomes higher compared with the surface layer owing to the simultaneous net surface heat loss, the temperature inversion can occur (Kurian and Vinayachandran, 2006; Girishkumar et al., 2013). The penetrated heat below the MLD is higher (mean $\sim 25 \text{ W/m}^2$) in the northern part of the Bay of Bengal throughout the year and lowest ($\sim 15 \text{ W/m}^2$) in winter (Figs 12b, e) due to lower incoming solar radiation during this season. Simultaneously, the net surface heat loss due to evaporation is highest during this season (Figs 7b, f), which significantly contributes to a reduced mixed layer temperature in this region. The mixed layer heat budget equation also depicts that mixed layer heat flux dominantly cools the mixed layer ($\sim -2.0^\circ\text{C}$) (Fig. 7i). The strong surface cooling along with the trapped heat ($\sim 15 \text{ W/m}^2$) in the subsurface forms a high ΔT , which has a positive correlation with ΔS ($r=0.77$; Fig. 8h). Notably, the amount of temperature inversion is less toward the southern part of the bay in this season, where the factors responsible for the formation of inversion are comparatively less favorable (Figs 7k, l). For instance, slight cooling tendency

($\sim -0.05^\circ\text{C}$) in the mixed layer and very small mixed layer salinity variation ($+0.02$) is observed in this part of the bay. The low net surface heat flux significantly corresponds ($r=-0.79$; Table 3) to the number of temperature inversion profiles, whereas positive E-P ($r=0.46$; Table 3) aids in reducing net surface heat flux in the Bay of Bengal. Therefore, based on the above discussion, the temperature inversion in the northern Bay of Bengal is dominantly controlled by the cooling tendency in the mixed layer due to net surface heat loss in winter. As horizontal advection of fresh-water-mediated stratification in winter is necessary to restrain evaporative cooling in shallow MLD regions, it is a prerequisite for the formation of temperature inversions. Similar mechanisms have been suggested for the formation of winter temperature inversions at RAMA buoy station located at 15°N , 90°E (Li et al., 2016; Thadathil et al., 2016). Moreover, penetrating heat below the shallow MLD aids in forming temperature inversion in this season. Remarkably, vertical processes (combination of vertical advection, entrainment, and diffusion in Eq. (3)) leads to warming tendency ($\sim 1.0^\circ\text{C}$) in the mixed layer along the northern bay during winter, which seems to explain the presence of temperature inversion as warm subsurface water can enter into the mixed layer through the entrainment and vertical diffusion.

During summer and autumn, the mixed layer salinity (29.5 to 33.5) is low, but the temperature remains comparatively higher than that in winter (29°C to 30.5°C), with dense temperature inversion profiles in the northern Bay of Bengal (Figs 6a, d, e, h).

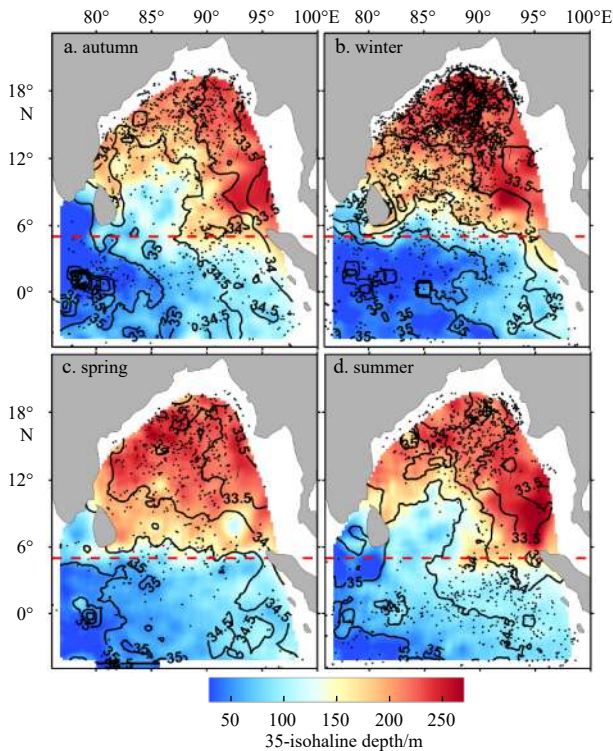


Fig. 9. Spatiotemporal distribution of the 35-isohaline depth overlaid with the salinity (contours) at 50-m depth, and occurrence of temperature inversion (black dots).

During these seasons, a large amount of freshwater from precipitation and river discharge spreads out in the bay (Figs 7c, h) and retains the mixed layer salinity low, which is obvious from the negative fresh-water flux (~ -1.2) of the mixed layer salt budget (Fig. 7j). Horizontal advection of low saline water owing to the southward East Indian Coastal Current (Figs 10a, d for surface currents, see Shetye et al. (1996), Srivastava et al. (2018) for the East Indian Coastal Current) might also decrease the mixed layer salinity (negative salinity advection; Fig. 7j). However, vertical processes bring salty water into the mixed layer and cannot dominate over the prevailing fresher water.

The 32.5-isohaline depth of the temperature inversion profile becomes deeper in this region during summer and autumn than in other seasons (Fig. 8a) and makes the upper layer strongly stratified with high ΔS (Figs 8c–f). During these seasons, the intruding salty Arabian Sea water remains at a comparatively shallower depth than other seasons inside the Bay of Bengal (Figs 10a, d) and may aid in strengthening ΔS . High ΔS supports a shallow MLD in this bay, but the MLD in summer is comparatively deeper than that in autumn because the wind turbulent kinetic energy is stronger in summer than in autumn (Figs 11a, d). Consequently, the penetrated heat below the MLD is higher in autumn (basin mean $\sim 25 \text{ W/m}^2$) than in summer ($\sim 18 \text{ W/m}^2$) because of the higher incoming solar radiation and shallower MLD during autumn (Fig. 12). Slight cooling tendency in the mixed layer is observed during these seasons and the negative mixed layer heat flux drives this cooling (Fig. 7i). However, cooling due to mixed layer heat loss is lower during autumn (-0.1°C) than summer (-0.3°C). The higher number of temperature inversion in autumn than in summer might be the consequence of higher penetrative heat below the MLD during autumn. Advection of cool low saline water (negative temperature advection) also tries

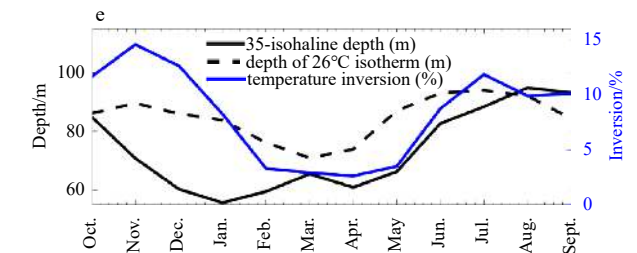
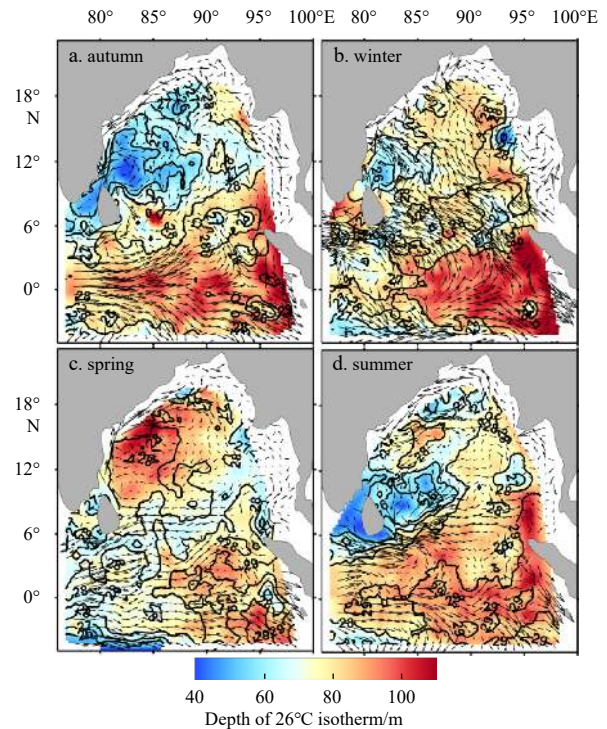


Fig. 10. Spatiotemporal distribution of the depth of 26°C isotherm overlaid with the temperature (contours) at 50-m depth, and surface current vectors (a–d), monthly variation of 35-isohaline depth, depth of 26°C isotherm, and temperature inversion profiles along the EEIO (e).

to decrease the mixed layer temperature in autumn. Hence, freshwater-mediated stratification controls the temperature inversion during these seasons through the high penetrative heat below the shallow MLD, and slight cooling tendency in the mixed layer. Notably, substantial warming in the mixed layer through vertical processes is observed during these seasons, and it becomes higher during autumn. The warming in the mixed layer during these seasons due to the presence of temperature inversion might have commensurable impact in shaping SST and thus, climate system through air-sea interaction.

Along the southern Bay of Bengal, salting tendency in summer and very small variation in salinity (~ 0.08) in autumn within the mixed layer are unfavorable to the formation of temperature inversion during these seasons (Fig. 7i). Although mixed layer fresh-water flux is negative, strong vertical processes bring saltier water from underneath and retains the mixed layer salinity high during these seasons. Moreover, during autumn fresh-water is horizontally advected from the northern bay, whereas during summer, advected saltier water originating from the Arabian Sea keeps the mixed layer salinity high in this part of the bay, which is evident from the direction of surface current (Figs 10a, d) as well

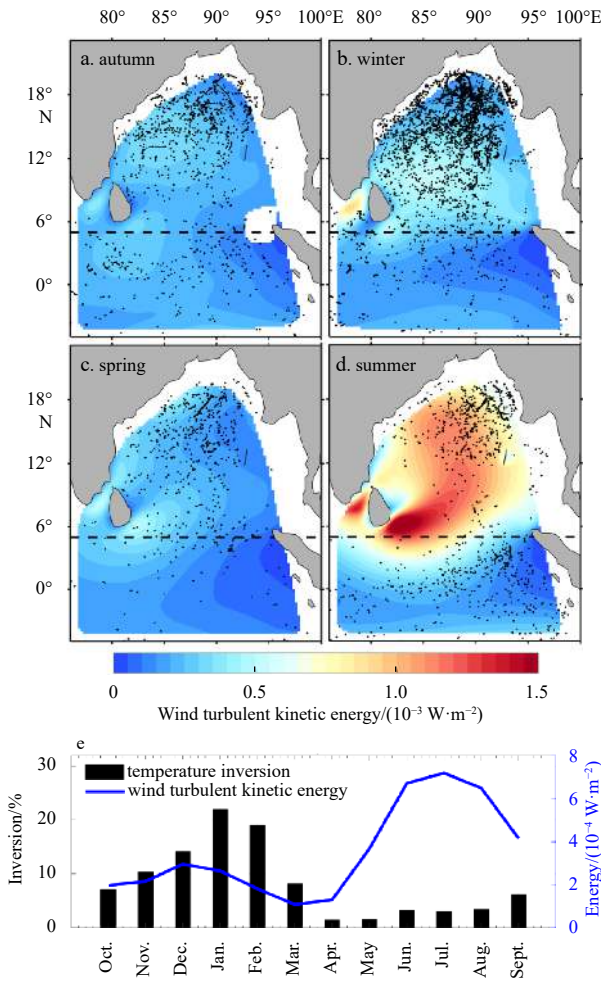


Fig. 11. Spatiotemporal distribution of the wind turbulent kinetic energy (a–d), and monthly variation in wind turbulent kinetic energy and temperature inversion (e).

as horizontal salinity advection term (Fig. 7l). High net surface heat flux warms the mixed layer in autumn (Fig. 7k). However, mixed layer exhibits cooling tendency during summer, which is driven by the strong vertical processes (Fig. 7k). For instance, upwelling along the Sri Lanka dome and western part of the bay, and the subsequent uplift of thermocline (26°C isotherm, Figs 10a, d) cools this mixed layer, which is also not much suitable to form temperature inversion in this part of the bay during summer and autumn.

During spring, the net surface heat flux is positive, and evaporation is dominant over precipitation in the Bay of Bengal (Figs 7c, g). Consequently, the positive heat flux and fresh-water flux (Figs 7i–l) keep both the mixed layer temperature and salinity higher than those in the other seasons. Additionally, the 32.5-isohaline depth of the temperature inversion profile occurs at the shallowest depth (basin mean ~ 18 m) in this season (Fig. 8a) when ΔS is also low (Figs 8e, g). However, in some areas of the northern Bay of Bengal, low mixed layer temperature (27°C to 29°C) and salinity (31.5 to 33.5) (Figs 6c, g) with few temperature inversion profiles are observed in this season. Thus, the seasonal mixed layer heat and salt budget cannot clearly explain the causes of this low mixed layer temperature and salinity during this period (Figs 7i–l). However, the highest incoming solar radi-

ation and thus, thermally stratified shallow MLD prevails in this season (Figs 12f, g). Consequently, the penetrated heat below the MLD is the highest (basin mean $\sim 28 \text{ W/m}^2$) (Figs 12c, e), and the wind turbulent kinetic energy is low along the northeastern part of the Bay of Bengal during this season, where some temperature inversion exists (Figs 11c, e). Thus, subsurface warming owing to penetrating heat and simultaneous cooling in the surface due to net surface heat loss for short period might produce such temperature inversion even during spring. Mechanisms of shorter time scales (e.g., strong wind and heat loss) might help to form short-lived temperature inversions (Thadathil et al., 2002).

3.2.2 The EEIO

The mixed layer temperature (29°C to 30.5°C) gradually increases towards the southern part of the Bay of Bengal and remains comparatively higher in the EEIO year-round (Figs 6a–h). Although the net surface heat flux exhibits positive values throughout the year (Figs 7a–d), slight cooling tendency in mixed layer is observed except during spring in this region (Fig. 7m). Mixed layer heat flux is high during spring (warms $\sim 0.3^\circ\text{C}$) but slightly lower in other seasons (cools $\sim 0.05^\circ\text{C}$) (Fig. 7m). This cooling in the mixed layer is advantageous in forming temperature inversion in the EEIO. Vertical processes exhibit a warming tendency in the mixed layer throughout the year except spring, and this warming is a little higher during summer and autumn ($\sim 0.08^\circ\text{C}$) than winter (Fig. 7m). Moreover, the warming owing to the vertical processes is also an indication of the formation of temperature inversion in the EEIO except in spring. However, the contribution of horizontal advection to mixed layer temperature is positive ($\sim 0.1^\circ\text{C}$) during autumn and spring (Fig. 7m). Direction of strong surface current during these seasons also exhibit the intrusion of warmer and saltier Arabian Sea water towards the EEIO (Figs 10a–d). Moreover, the MLD is deeper in the EEIO than in the Bay of Bengal (De Boyer Montégut et al., 2007), and the penetrated heat below the deep MLD is also lower (Figs 12a–d). Thus, horizontal advection and penetrated heat cannot significantly contribute to the temperature inversion.

Precipitation dominates over evaporation along the EEIO and the southern Bay of Bengal all year round, and comparatively higher precipitation occurs during summer and autumn (Figs 7e–h; Qu and Meyers, 2005; De Boyer Montégut, et al., 2007). The negative fresh-water flux (decreases in mixed layer salinity by ~ 0.2) throughout the year and negative horizontal advection of low salinity water during summer to the subsequent winter also support the occurrence of high precipitation in the EEIO (Fig. 7n). However, small salinity variation (~ 0.1) in the mixed layer prevails during summer to subsequent winter, which seems to be reduced by the salting tendency due to vertical processes. Thus, the spatiotemporal correlation between precipitation and dense temperature inversion depicts that precipitation could be a favorable factor for the formation of temperature inversion in the EEIO, especially during summer and autumn. The low wind turbulent kinetic energy is also spatially strongly correlated with the dense temperature inversion in the EEIO (Fig. 11), although basin-wide correlation between them is moderate ($r = -0.42$; Table 3).

Comparatively higher (than northern bay) mixed layer temperature and salinity in the EEIO might be retained in the mixed layer by the intrusion of warm-salty water from the Arabian Sea (Figs 9 and 10). If this warm-salty water can subduct below the MLD, then it would be favorable to the formation of temperature inversion. Notably, MLD is approximately 30 m to 90 m deep along the EEIO and becomes deeper towards the eastern side (Fig. 13). From winter to spring, the intrusion of salty water is

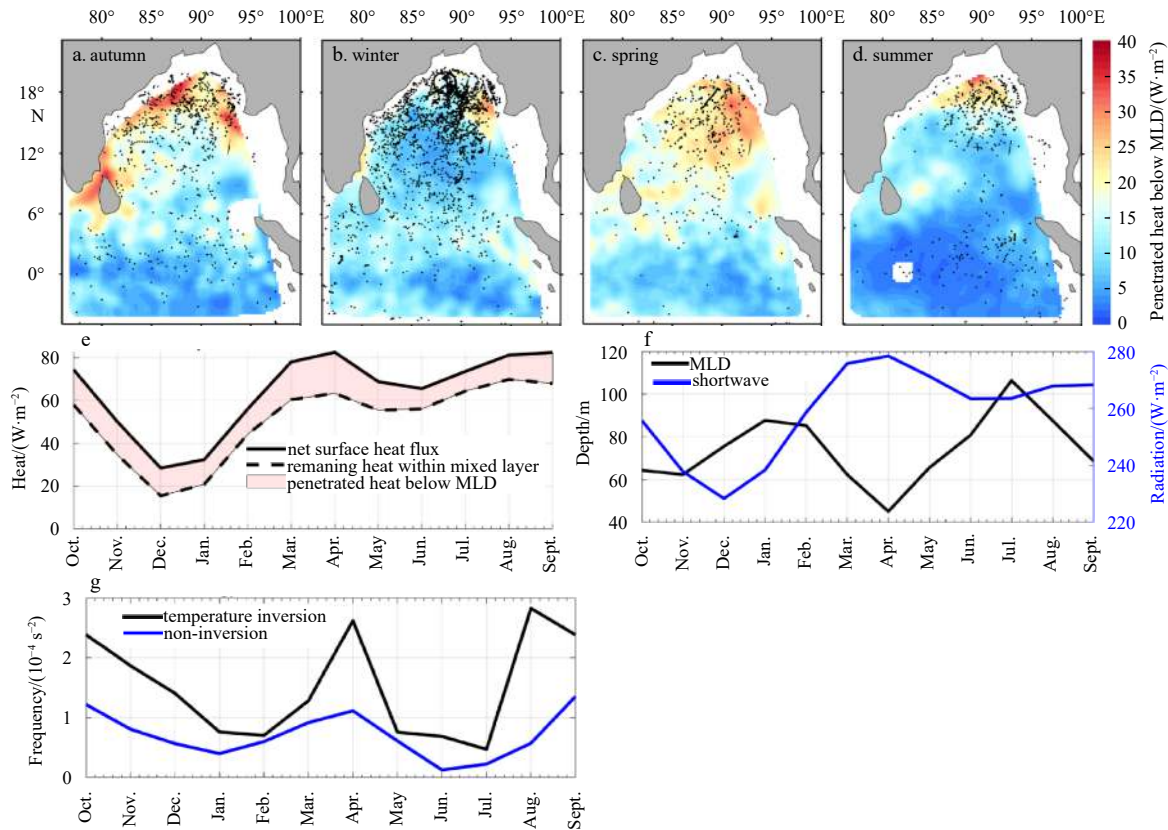


Fig. 12. Spatial distribution of the amount of heat penetrated below mixed layer depth (MLD) (a–d), monthly distribution of the amount of heat penetrated below MLD (e), MLD in temperature inversion profiles, and incoming shortwave radiation (f), and stratification in the surface water (g).

eastward along the EEIO, and 35-isohaline remains at a shallow depth (~ 65 m) in this region (Figs 9b, c). As the salty water pumps up toward the surface, it increases the surface salinity in this region (as observed from the mixed layer salinity and salinity at 50 m depth), where a smaller number of temperature inversions is observed. However, from summer to autumn, the direction of 35-isohaline extends northward into the Bay of Bengal and is retained at comparatively shallow depths along its path (Figs 9a, d). However, at the same time, the salty water enters into the deeper depth (~ 90 m) (sliding toward the subsurface), creating a frontal zone along the eastern side of the EEIO where the number of temperature inversions is comparatively higher. Depth of 26°C isotherm also shows that the thermocline is deeper along the EEIO during summer and autumn than other seasons where temperature inversions are denser (Fig. 10). The 35-isohaline depth also depicts that the deeper the depth of salty intruding Arabian Sea water, the higher the number of temperature inversion profiles along the EEIO (Fig. 10e). Additionally, the north-south gradient of mixed layer temperature (Figs 6a–d) and temperature at 50-m depth (Figs 10a–d, contours) indicate that the Arabian Sea water is warmer than the Bay of Bengal water. Thus, sliding of the warm-salty water toward the subsurface (below the MLD) creates a vertical thermohaline gradient, which is important to form the temperature inversion in the EEIO mainly during summer and autumn. Besides, deepening of thermocline and co-occurrence of atmospheric heat loss induced slight cooling tendency in the mixed layer assists the formation of temperature inversions in this region. The subduction of warm-salty water below the fresher colder water-generated thermohaline front is also

reported to be an important source of temperature inversion in the western Pacific Ocean (Nagata, 1970; Ueno et al., 2005) and in the southeastern Arabian Sea (Thadathil and Gosh, 1992; Shankar et al., 2004; Durand et al., 2004; Kurian and Vinayachandran, 2006).

During summer and autumn, both the initial inversion depth and depth of peak temperature in the temperature inversion profiles are deeper along the EEIO and the eastern side of the Bay of Bengal (Figs 5k, l). From their distribution, it seems that temperature inversion follows a propagation feature from the EEIO to the eastern side of the Bay of Bengal. Distribution of the depth of 26°C isotherm during summer and autumn also exhibit similar downwelling propagation signature (Figs 10a, d). This propagation might be the signature of the downwelling Rossby wave (Qu and Meyers, 2005; Rao et al., 2010; Girishkumar et al., 2011), which is reported as a cause of temperature inversion in this region by Thompson et al. (2006). As downwelling Rossby waves deepen the thermocline (Yu, 2003), which slides below the comparatively colder and fresher surface water from the Bay of Bengal, temperature inversion can occur in these areas (Thompson et al., 2006; Girishkumar et al., 2013).

3.3 Causes of seasonal variations of characteristics of temperature inversion

Temperature inversion layer usually lies above the thermocline layers (De Boyer Montégut et al., 2007; Thadathil et al., 2016; Shee et al., 2019). It is found that a shallow MLD and thus a thick barrier layer corresponds with the thick layer of inversion (Masson et al., 2002; De Boyer Montégut et al., 2007; Thadathil et

al., 2016). He et al. (2020) has also reported that winter temperature inversion in the northern Bay of Bengal depends on the downwelling tendency of eddy and consequent thick barrier layer. Hence, seasonal variations of the characteristics of the temperature inversion: initial inversion depth, depth of peak temperature, and thickness of inversion layer might be related to the variations in MLD, ILD, and barrier layer thickness (BLT), and thus is addressed in this section (Fig. 13).

The spatial distribution of MLD demonstrates a good relationship ($r=0.54$, 95% significant) with initial inversion depth (Figs 13a–d). MLD ranges from 10 m to 90 m, while initial inversion depth varies within 10 m to 50 m depth in the study domain. Both of them show a strong seasonal variation. MLD and the initial inversion depth exhibit a strong north-south gradient with remarkably shallow depth along the northern Bay of Bengal, as freshwater-mediated high ΔS (haline stratification) is prominent there. On the other hand, comparatively deeper MLD and initial inversion depth are seen along the southern bay (south of 15°N) where ΔT and ΔS are small. They are deeper in the EEIO regions where salty and denser Arabian Sea water (Vinayachandran et al., 2013) retain almost the year-round. They are also deeper in

the southwestern bay in summer and in the central bay in winter where salinity is enhanced by strong monsoonal wind (Shetye et al., 1996; Srivastava et al., 2018) mediated mixing. However, during spring and autumn, due to strong thermal stratification (Kumari et al., 2018) they become shallow. Hence, this study suggests that the initial inversion depth of temperature inversion profile greatly depends on MLD and its associated factors. Remarkably, temperature inversions forms along the northern Bay of Bengal where MLD is shallow, and along EEIO where MLD is deep. Thus, inversion obviously forms in both the shallow and deep MLD regions in this study area. However, previously reported temperature inversion is only in shallow MLD region along the northern Bay of Bengal where strong haline stratification exists (De Boyer Montégut et al., 2007; Thadathil et al., 2016; Li et al., 2016).

Spatial distribution exhibits that the deeper the ILD, the deeper the depth of peak temperature throughout the study domain (Figs 13e–h), and they have a strong correlation ($r=0.71$). Notably, ILD remains always deeper than that of the depth of peak temperature. The spatial distribution of the seasonal variation of depth of peak temperature and ILD mostly follows the

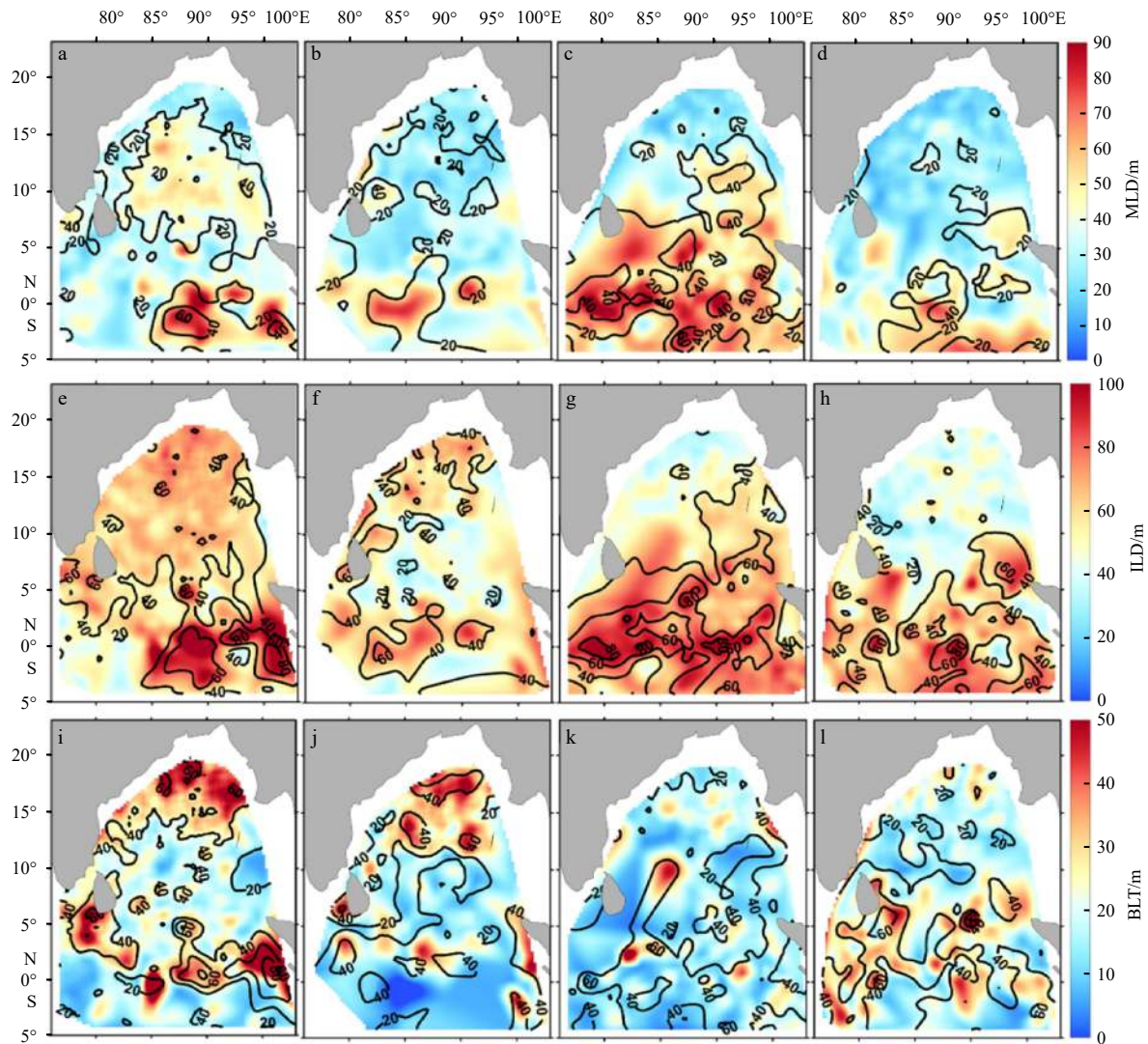


Fig. 13. Season-wise spatial distribution of mixed layer depth (MLD) (shading) overlaid with contours of initial inversion depth (a–d), isothermal layer depth (ILD) (shading) with contours of depth of peak temperature (e–h), and barrier layer thickness (BLT) (shading) with the contours of thickness of inversion layer (i–l).

pattern of MLD and thus, salinity, stratification, and wind forcing also regulate them identical to MLD. Moreover, thicker temperature inversion along the northern Bay of Bengal during winter and along EEIO throughout the year co-occurs with the deeper ILD. Therefore, it can be stated that the deeper ILD can be an indicator of deeper depth of peak temperature and intense inversion.

The thickness of inversion layer and BLT have similar spatiotemporal distribution (Figs 13i–l) with a strong correlation ($r=0.63$) throughout the year. Notably, inversion layer is always thicker (basin mean ~ 6 m thicker) than the barrier layer as initial inversion depth is shallower than MLD. Thickness of inversion layer and BLT are the highest in winter along the northern bay where the occurrence of temperature inversion and ΔT are the highest. They are also high along the east part of the EEIO region in the year-round where occurrence of inversions is also high. However, they are low in spring throughout the bay, and along the northern bay during summer and autumn where ILD and MLD are also comparatively shallow (Fig. 13). Therefore, deeper ILD, and thicker BLT promote to form an intense temperature inversion both in the Bay of Bengal and EEIO.

4 Summary and conclusions

Occurrence of temperature inversion during winter in the northern Bay of Bengal is reported earlier. However, the detailed spatial and temporal information of the temperature inversion in the entire bay throughout the year is a question yet to be answered. The objective of this study is to analyze each quality-controlled Argo profile (39 293 in number) over a period of 17 years (2004 to 2020) to draw a detailed picture of the spatiotemporal distribution of temperature inversion along with its causative factors in the Bay of Bengal and the adjacent EEIO, which is summarized in a schematic figure (Fig. 14). Another available observational data sources in the study domain, RAMA buoys (total eight buoys with 28 894 number of daily profiles) over the year 2007 to 2020 are also incorporated in this study.

Considering the threshold of 0.2°C , 17.5% of the total Argo and 51.6% of RAMA profiles are found to have temperature inversions in the study domain. Both of these data sources exhibit that temperature inversion occurs year-round in the entire Bay of Bengal and the EEIO. Occurrence of temperature inversion (approximately 50% of the total inversion profiles) is the highest during winter and the lowest during spring ($\sim 12\%$). During summer and autumn, the percentages of temperature inversion profiles are $\sim 18\%$ and $\sim 20\%$, respectively. Besides the frequent inversion in winter season in the Bay of Bengal, existence of the finer scale temperature inversion along the Bay of Bengal and EEIO during summer and autumn is reported in this study for the first time. Seasonal variation in temperature inversion (standard deviation $\sim 7\%$) is stronger than that of inter-annual (4.1%).

The basin-wide mean ΔT ranges 0.2°C to 1.4°C year-round, but it exceeds 4°C during winter in the northern Bay of Bengal. The depth of peak temperature ranges from ~ 30 m to 90 m and thickness of inversion layer from ~ 20 m to 80 m, and both of them are higher along the equatorial region and decrease gradually northward.

The current study has extensively discussed and separated the driving processes of temperature inversion for the northern Bay of Bengal, southern Bay of Bengal, and EEIO. Mechanisms reported in this study except for the northern bay during winter seems to be novel findings. Salt budget analysis for the northern Bay of Bengal reveals the high freshening tendency in the mixed layer due to negative fresh-water flux and advection of ample prevailing fresher water all the year round, and retains the no-

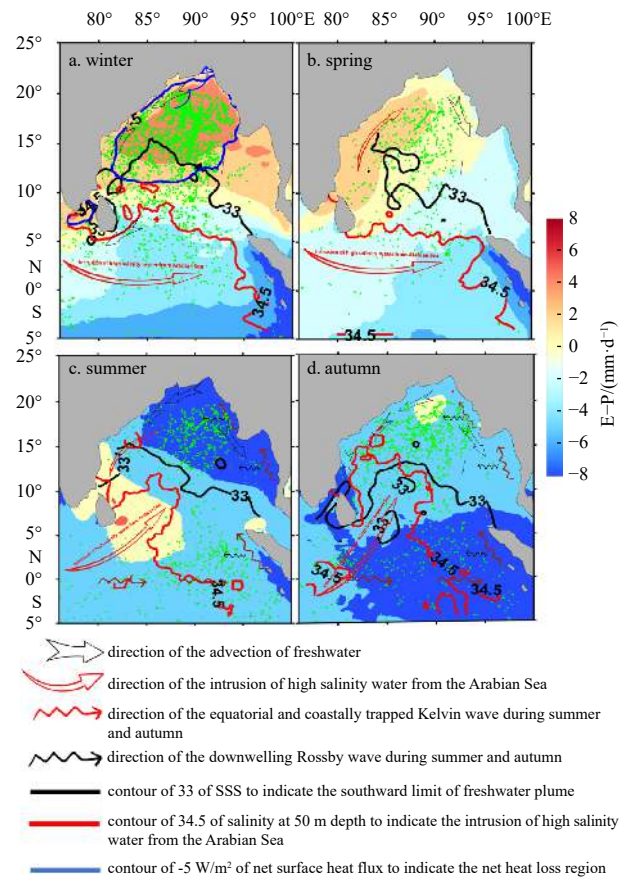


Fig. 14. A sketch of the spatiotemporal distribution and dominant formation mechanisms of temperature inversion in the Bay of Bengal and EEIO. Green dots refer to the location of temperature inversion profiles.

ticeable shallow MLD. Considerable amount of short-wave radiation (mean ~ 25 W/m^2) can reach below this shallow MLD and warms the subsurface. Besides, extensive cooling tendency in the mixed layer is observed from heat budget analysis except spring season. Therefore, co-occurrence of relatively warmer subsurface layer and cooler mixed layer dominantly controls the existence of temperature inversion in this part of the bay almost throughout the year. Remarkably, vertical processes through the entrainment and vertical diffusion exhibits obvious warming tendency in the mixed layer along the northern bay during winter, summer and autumn. These vertical processes due to the presence of temperature inversion might have commensurable impact in shaping SST and thus, climate system through air-sea interaction.

In the southern Bay of Bengal, cooling tendency in the mixed layer is observed due to the low mixed layer heat flux only during summer and barely during winter. In contrast to the northern bay, vertical processes cool the mixed layer throughout the year and aforesaid cooling is less suitable in forming temperature inversion. However, the negative mixed layer fresh-water flux is compensated by the vertical processes to some extent, which eventually retains the weaker mixed layer salinity tendency, which is also less favorable for inversion in this region than northern part of the bay. Therefore, less cooling as well as high salinity in the mixed layer prevent to form temperature inversion in the southern Bay of Bengal throughout the year.

In the EEIO, high precipitation retains the mixed layer fresh-

water flux negative, but salting by the vertical processes compensate some of this low salinity water, even though, mixed layer salinity tendency becomes little fresher except spring. Besides, slightly cooling tendency in the mixed layer due to the atmospheric heat loss favors in forming temperature inversion during summer and autumn, and a bit warming by the vertical processes also give the evidence of the existence of comparatively warmer water below the MLD than the mixed layer. Remarkably, deeper thermocline layer, and the sliding of warm-salty Arabian Sea water (>35) beneath the cold-fresher Bay of Bengal water might increase temperature inversion during summer and autumn than other seasons in EEIO. Notably, remainder term derived from the mixed layer heat- and salt-budget analyses in this study might contain some uncertainties due to different errors including sampling and computational inaccuracy, and further quantification of the described mechanisms demands a dedicated modeling approach based on observations in future attempts.

Deeper ILD, and thicker BLT are spatially well correlated with the deeper depth of peak temperature and thicker inversion layer, respectively in the study area. Thus, they can be the indicators of intense inversion. Temperature inversions along the northern Bay of Bengal co-occurs with shallow MLD, and along the EEIO with deep MLD. Thus, inversion obviously can form in both the shallow and deep MLD regions, although it is previously reported only in shallow MLD regions.

Although temperature inversion and noninversion have their own favorable zones and times, they occur simultaneously throughout the study area. In some regions, the temperature and salinity may be more favorable for noninversion, but the temperature inversion may also occur on a short time and small spatial scale. However, the occurrence of those comparatively small-scale inversions might influence some mesoscale events, such as tropical cyclones and eddies. This is worth studying in detail in the future by utilizing high temporal resolution (e.g., hourly) observational data.

Acknowledgements

This research was possible owing to the free availability of the Argo temperature and salinity profile of Argo Global Data Access Experiment Center. The authors would also like to thank the detailed and constructive comments from the two anonymous reviewers that guided the revision of the original manuscript.

References

- Akhil V P, Durand F, Lengaigne M, et al. 2014. A modeling study of the processes of surface salinity seasonal cycle in the Bay of Bengal. *Journal of Geophysical Research: Oceans*, 119(6): 3926–3947, doi: [10.1002/2013JC009632](https://doi.org/10.1002/2013JC009632)
- Argo. 2021. Argo float data and metadata from Global Data Assembly Centre (Argo GDAC). Plouzané: SEANO, doi: [10.17882/42182](https://doi.org/10.17882/42182)
- Balaguru K, Chang Ping, Saravanan R, et al. 2012. Ocean barrier layers' effect on tropical cyclone intensification. *Proceedings of the National Academy of Sciences of the United States of America*, 109(36): 14343–14347, doi: [10.1073/pnas.1201364109](https://doi.org/10.1073/pnas.1201364109)
- Chaitanya A V S, Lengaigne M, Vialard J, et al. 2014. Salinity measurements collected by fishermen reveal a “River in the Sea” flowing along the eastern coast of India. *Bulletin of the American Meteorological Society*, 95(12): 1897–1908, doi: [10.1175/BAMS-D-12-00243.1](https://doi.org/10.1175/BAMS-D-12-00243.1)
- Chowdhury K M A, Jiang Wensheng, Liu Guimei, et al. 2019. Formation and types of thermal inversion in the Bay of Bengal. *CLIVAR Exchanges*, 76: 20–23
- Chowdhury K M A, Mahbub-E-Kibria A S M, Akhter S, et al. 2017. Variation of water column density in the Bay of Bengal aquatic ecosystem. *International Journal of Fisheries and Aquatic Studies*, 5(6): 34–40
- De Boyer Montégut C, Madec G, Fischer A S, et al. 2004. Mixed layer depth over the global ocean: An examination of profile data and a profile-based climatology. *Journal of Geophysical Research: Oceans*, 109(C12): C12003, doi: [10.1029/2004jc002378](https://doi.org/10.1029/2004jc002378)
- De Boyer Montégut C, Mignot J, Lazar A, et al. 2007. Control of salinity on the mixed layer depth in the world ocean: 1. general description. *Journal of Geophysical Research: Oceans*, 112(C6): C06011, doi: [10.1029/2006JC003953](https://doi.org/10.1029/2006JC003953)
- Durand F, Shetye S R, Vialard J, et al. 2004. Impact of temperature inversions on SST evolution in the South-Eastern Arabian Sea during the pre-summer monsoon season. *Geophysical Research Letters*, 31(1): L01305, doi: [10.1029/2003GL018906](https://doi.org/10.1029/2003GL018906)
- Foltz G R, McPhaden M J. 2009. Impact of barrier layer thickness on SST in the central tropical North Atlantic. *Journal of Climate*, 22(2): 285–299, doi: [10.1175/2008JCLI2308.1](https://doi.org/10.1175/2008JCLI2308.1)
- Girishkumar M S, Ravichandran M, McPhaden M J. 2013. Temperature inversions and their influence on the mixed layer heat budget during the winters of 2006–2007 and 2007–2008 in the Bay of Bengal. *Journal of Geophysical Research: Oceans*, 118(5): 2426–2437, doi: [10.1002/jgrc.20192](https://doi.org/10.1002/jgrc.20192)
- Girishkumar M S, Ravichandran M, McPhaden M J, et al. 2011. Intraseasonal variability in barrier layer thickness in the south central Bay of Bengal. *Journal of Geophysical Research: Oceans*, 116(C3): C03009, doi: [10.1029/2010JC006657](https://doi.org/10.1029/2010JC006657)
- Godfrey J S, Lindstrom E J. 1989. The heat budget of the equatorial western Pacific surface mixed layer. *Journal of Geophysical Research: Oceans*, 94(C6): 8007–8017, doi: [10.1029/JC094iC06p08007](https://doi.org/10.1029/JC094iC06p08007)
- Halkides D, Lee T. 2011. Mechanisms controlling seasonal mixed layer temperature and salinity in the southwestern tropical Indian Ocean. *Dynamics of Atmospheres and Oceans*, 51(3): 77–93, doi: [10.1016/j.dynatmoce.2011.03.002](https://doi.org/10.1016/j.dynatmoce.2011.03.002)
- He Qingyou, Zhan Haigang, Cai Shuqun. 2020. Anticyclonic eddies enhance the winter barrier layer and surface cooling in the Bay of Bengal. *Journal of Geophysical Research: Oceans*, 125(10): e2020JC016524, doi: [10.1029/2020JC016524](https://doi.org/10.1029/2020JC016524)
- Kara A B, Rochford P A, Hurlburt H E. 2000. Mixed layer depth variability and barrier layer formation over the North Pacific Ocean. *Journal of Geophysical Research: Oceans*, 105(C7): 16783–16801, doi: [10.1029/2000JC900071](https://doi.org/10.1029/2000JC900071)
- Kashem M, Ahmed M K, Qiao Fangli, et al. 2019. The response of the upper ocean to tropical cyclone Viyaru over the Bay of Bengal. *Acta Oceanologica Sinica*, 38(1): 61–70, doi: [10.1007/s13131-019-1370-1](https://doi.org/10.1007/s13131-019-1370-1)
- Kumari A, Kumar S P, Chakraborty A. 2018. Seasonal and interannual variability in the barrier layer of the Bay of Bengal. *Journal of Geophysical Research: Oceans*, 123(2): 1001–1015, doi: [10.1002/2017JC013213](https://doi.org/10.1002/2017JC013213)
- Kurian J, Vinayachandran P N. 2006. Formation mechanisms of temperature inversions in the southeastern Arabian Sea. *Geophysical Research Letters*, 33(17): L17611, doi: [10.1029/2006GL027280](https://doi.org/10.1029/2006GL027280)
- Li Kuiping, Wang Haiyuan, Yang Yang, et al. 2016. Observed characteristics and mechanisms of temperature inversion in the northern Bay of Bengal. *Haiyang Xuebao*, 38(7): 22–31
- Li Jian, Yang Lei, Shu Yeqiang, et al. 2012. Temperature inversion in the Bay of Bengal prior to the summer monsoon onsets in 2010 and 2011. *Atmospheric and Oceanic Science Letters*, 5(4): 290–294, doi: [10.1080/16742834.2012.11447004](https://doi.org/10.1080/16742834.2012.11447004)
- Luis A J, Kawamura H. 2000. Wintertime wind forcing and sea surface cooling near the south India tip observed using NSCAT and AVHRR. *Remote Sensing of Environment*, 73(1): 55–64, doi: [10.1016/S0034-4257\(00\)00081-X](https://doi.org/10.1016/S0034-4257(00)00081-X)
- Ma Tian, Qi Yiquan, Cheng Xuhua. 2019. Intraseasonal-to-semiannual variability of barrier layer thickness in the eastern equatorial Indian Ocean and Bay of Bengal. *Journal of Tropical Oceanography*, 38(5): 18–31
- Masson S, Delecluse P, Boulanger J P, et al. 2002. A model study of the seasonal variability and formation mechanisms of the barrier

- er layer in the eastern equatorial Indian Ocean. *Journal of Geophysical Research: Oceans*, 107(C12): 8017, doi: [10.1029/2001JC000832](https://doi.org/10.1029/2001JC000832)
- Mignot J, Lazar A, Lacarra M. 2012. On the formation of barrier layers and associated vertical temperature inversions: a focus on the northwestern tropical Atlantic. *Journal of Geophysical Research: Oceans*, 117(C2): C02010, doi: [10.1029/2011JC007435](https://doi.org/10.1029/2011JC007435)
- Monterey G I, Levitus S. 1997. *Seasonal Variability of Mixed Layer Depth for the World Ocean*. Silver Spring: NOAA
- Morel A, Antoine D. 1994. Heating rate within the upper ocean in relation to its bio-optical state. *Journal of Physical Oceanography*, 24(7): 1652–1665, doi: [10.1175/1520-0485\(1994\)024<1652:HR-WTUO>2.0.CO;2](https://doi.org/10.1175/1520-0485(1994)024<1652:HR-WTUO>2.0.CO;2)
- Nagata Y. 1970. Detailed temperature cross section of the cold-water belt along the northern edge of the Kuroshio. *Journal of Marine Research*, 28(1): 1–14
- Pant V, Girishkumar M S, Bhaskar T V S U, et al. 2015. Observed inter-annual variability of near-surface salinity in the Bay of Bengal. *Journal of Geophysical Research: Oceans*, 120(5): 3315–3329, doi: [10.1002/2014JC010340](https://doi.org/10.1002/2014JC010340)
- Qu Tangdong, Meyers G. 2005. Seasonal variation of barrier layer in the southeastern tropical Indian Ocean. *Journal of Geophysical Research: Oceans*, 110(C11): C11003, doi: [10.1029/2004JC002816](https://doi.org/10.1029/2004JC002816)
- Rao B P, Babu V R, Chandramohan P. 1987. Seasonal and diurnal variability of thermal structure in the coastal waters off Visakhapatnam. *Proceedings of the Indian Academy of Sciences-Earth and Planetary Sciences*, 96(1): 69–79, doi: [10.1007/BF02842639](https://doi.org/10.1007/BF02842639)
- Rao R R, Kumar M S G, Ravichandran M, et al. 2010. Interannual variability of Kelvin wave propagation in the wave guides of the equatorial Indian Ocean, the coastal Bay of Bengal and the southeastern Arabian Sea during 1993–2006. *Deep-Sea Research Part I: Oceanographic Research Papers*, 57(1): 1–13, doi: [10.1016/j.dsr.2009.10.008](https://doi.org/10.1016/j.dsr.2009.10.008)
- Rao R R, Rao D S, Murthy P G K, et al. 1983. A preliminary investigation of the summer monsoonal forcing on the thermal structure of upper Bay of Bengal during Monex-79. *Mausum*, 32: 85–92
- Rao R R, Sivakumar R. 2003. Seasonal variability of sea surface salinity and salt budget of the mixed layer of the north Indian Ocean. *Journal of Geophysical Research: Oceans*, 108(C1): 3009, doi: [10.1029/2001JC000907](https://doi.org/10.1029/2001JC000907)
- Roseli N H, Akhira M F, Husain M L, et al. 2015. Water mass characteristics and stratification at the shallow Sunda Shelf of southern South China Sea. *Open Journal of Marine Science*, 5(4): 455–467, doi: [10.4236/ojms.2015.54036](https://doi.org/10.4236/ojms.2015.54036)
- Schiller A, Godfrey J S. 2003. Indian Ocean intraseasonal variability in an ocean general circulation model. *Journal of Climate*, 16(1): 21–39, doi: [10.1175/1520-0442\(2003\)016<0021:IOVIA>2.0.CO;2](https://doi.org/10.1175/1520-0442(2003)016<0021:IOVIA>2.0.CO;2)
- Shankar D, Gopalakrishna V V, Shenoi S S C, et al. 2004. Observational evidence for westward propagation of temperature inversions in the southeastern Arabian Sea. *Geophysical Research Letters*, 31(8): L08305, doi: [10.1029/2004GL019652](https://doi.org/10.1029/2004GL019652)
- Shankar D, Remya R, Vinayachandran P N, et al. 2016. Inhibition of mixed-layer deepening during winter in the northeastern Arabian Sea by the West India Coastal Current. *Climate Dynamics*, 47(3–4): 1049–1072, doi: [10.1007/s00382-015-2888-3](https://doi.org/10.1007/s00382-015-2888-3)
- Shee A, Sil S, Gangopadhyay A, et al. 2019. Seasonal evolution of oceanic upper layer processes in the northern Bay of Bengal following a single Argo float. *Geophysical Research Letters*, 46(10): 5369–5377, doi: [10.1029/2019GL082078](https://doi.org/10.1029/2019GL082078)
- Shetye S R, Gouveia A D, Shankar D, et al. 1996. Hydrography and circulation in the western Bay of Bengal during the northeast monsoon. *Journal of Geophysical Research: Oceans*, 101(C6): 14011–14025, doi: [10.1029/95JC03307](https://doi.org/10.1029/95JC03307)
- Shetye S R, Gouveia A D, Shenoi S S C, et al. 1993. The western boundary current of the seasonal subtropical gyre in the Bay of Bengal. *Journal of Geophysical Research: Oceans*, 98(C1): 945–954, doi: [10.1029/92JC02070](https://doi.org/10.1029/92JC02070)
- Sprintall J, Tomczak M. 1992. Evidence of the barrier layer in the surface layer of the tropics. *Journal of Geophysical Research: Oceans*, 97(C5): 7305–7316, doi: [10.1029/92JC00407](https://doi.org/10.1029/92JC00407)
- Srivastava A, Dwivedi S, Mishra A K. 2018. Investigating the role of air-sea forcing on the variability of hydrography, circulation, and mixed layer depth in the Arabian Sea and Bay of Bengal. *Oceanologia*, 60(2): 169–186, doi: [10.1016/j.oceano.2017.10.001](https://doi.org/10.1016/j.oceano.2017.10.001)
- Suryanarayana A, Murty V S N, Rao D P. 1993. Hydrography and circulation of the Bay of Bengal during early winter, 1983. *Deep-Sea Research Part I: Oceanographic Research Papers*, 40(1): 205–217, doi: [10.1016/0967-0637\(93\)90061-7](https://doi.org/10.1016/0967-0637(93)90061-7)
- Sweeney C, Gnanadesikan A, Griffies S M, et al. 2005. Impacts of shortwave penetration depth on large-scale ocean circulation and heat transport. *Journal of Physical Oceanography*, 35(6): 1103–1119, doi: [10.1175/JPO2740.1](https://doi.org/10.1175/JPO2740.1)
- Thadathil P, Gopalakrishna V V, Muraleedharan P M, et al. 2002. Surface layer temperature inversion in the Bay of Bengal. *Deep-Sea Research Part I: Oceanographic Research Papers*, 49(10): 1801–1818, doi: [10.1016/S0967-0637\(02\)00044-4](https://doi.org/10.1016/S0967-0637(02)00044-4)
- Thadathil P, Gosh A K. 1992. Surface layer temperature inversion in the Arabian Sea during winter. *Journal of Oceanography*, 48(3): 293–304, doi: [10.1007/BF02233989](https://doi.org/10.1007/BF02233989)
- Thadathil P, Muraleedharan P M, Rao R R, et al. 2007. Observed seasonal variability of barrier layer in the Bay of Bengal. *Journal of Geophysical Research: Oceans*, 112(C2): C02009, doi: [10.1029/2006JC003651](https://doi.org/10.1029/2006JC003651)
- Thadathil P, Suresh I, Gautham S, et al. 2016. Surface layer temperature inversion in the Bay of Bengal: main characteristics and related mechanisms. *Journal of Geophysical Research: Oceans*, 121(8): 5682–5696, doi: [10.1002/2016JC011674](https://doi.org/10.1002/2016JC011674)
- Thompson B, Gnanaseelan C, Salvekar P S. 2006. Seasonal evolution of temperature inversions in the north Indian Ocean. *Current Science*, 90(5): 697–704
- Ueno H, Oka E, Suga T, et al. 2005. Seasonal and interannual variability of temperature inversions in the subarctic North Pacific. *Geophysical Research Letters*, 32(20): L20603, doi: [10.1029/2005GL023948](https://doi.org/10.1029/2005GL023948)
- Vialard J, Delecluse P. 1998. An OGCM study for the TOGA decade. Part II: barrier-Layer formation and variability. *Journal of Physical Oceanography*, 28(6): 1089–1106, doi: [10.1175/1520-0485\(1998\)028<1089:AOSFTT>2.0.CO;2](https://doi.org/10.1175/1520-0485(1998)028<1089:AOSFTT>2.0.CO;2)
- Vialard J, Foltz G R, McPhaden M J, et al. 2008. Strong Indian Ocean sea surface temperature signals associated with the Madden-Julian Oscillation in late 2007 and early 2008. *Geophysical Research Letters*, 35(19): L19608, doi: [10.1029/2008GL035238](https://doi.org/10.1029/2008GL035238)
- Vinayachandran P N, Murty V S N, Babu V R. 2002. Observations of barrier layer formation in the Bay of Bengal during summer monsoon. *Journal of Geophysical Research: Oceans*, 107(C12): 8018, doi: [10.1029/2001JC000831](https://doi.org/10.1029/2001JC000831)
- Vinayachandran P N, Shankar D, Vernekar S, et al. 2013. A summer monsoon pump to keep the Bay of Bengal salty. *Geophysical Research Letters*, 40(9): 1777–1782, doi: [10.1002/grl.50274](https://doi.org/10.1002/grl.50274)
- Wong A, Keeley R, Carval T, et al. 2021. Argo quality control manual for CTD and trajectory data. <https://archimer.ifremer.fr/doc/00228/33951/32470.pdf> [2021-05-11/2021-06-20]
- Wyrtki K, Bennett E B, Rochford D J. 1971. *Oceanographic Atlas of the International Indian Ocean Expedition*. Washington: National Science Foundation, 531
- Yu Lisan. 2003. Variability of the depth of the 20°C isotherm along 6°N in the Bay of Bengal: its response to remote and local forcing and its relation to satellite SSH variability. *Deep-Sea Research Part II: Topical Studies in Oceanography*, 50(12–13): 2285–2304, doi: [10.1016/S0967-0645\(03\)00057-2](https://doi.org/10.1016/S0967-0645(03)00057-2)